2009

Laser assisted friction stir welding: finite volume method and metaheuristic optimization

Shivani Daftardar
Louisiana State University and Agricultural and Mechanical College, shivani.daftardar@gmail.com

LASER ASSISTED FRICTION STIR WELDING: FINITE VOLUME METHOD AND METAHEURISTIC OPTIMIZATION

A Thesis

Submitted to the Graduate Faculty of the
Louisiana State University and
Agricultural and Mechanical College
in partial fulfillment of the
requirements for the degree of
Master of Science in Industrial Engineering

in

The Department of Construction Management and Industrial Engineering

by
Shivani Daftardar
B.E, Maharashtra Institute of Technology, India, 2005
May 2009

Acknowledgments

I would like to acknowledge Dr T. Warren Liao, my graduate advisor and committee chairman, under whose supervision I chose this topic and began the thesis. Without his support and guidance, this work would not have been possible. I would also like to extend my sincere gratitude to the committee members Dr. Muhammad Wahab and Dr. Xiaoyue Jiang for agreeing to be part of my thesis defense and for their comments and inputs in my work.

I would also like to take this opportunity to gratefully acknowledge my friend, Kedar Jathar, who has been abundantly helpful in numerous ways. I am much indebted to him for his valuable assistance in learning FLUENT. I have deeply benefitted from his knowledge and advice.

I cannot end without once again thanking Dr T. Warren Liao for his unflinching support and guidance, throughout the course of my study and research. I will always be grateful to him in every possible way. Last but not the least I am also thankful to my friends and family for supporting me and encouraging me to pursue this degree.

Table of Contents

List of Tables

List of Figures

Abstract

Friction Stir Welding (FSW) is a solid state joining process that uses a non-consumable rotating welding tool to generate frictional heat at the welding location. Large forces are required to produce friction between the welding tool and the work piece which increases the wear rate of the welding tool in welding materials with high melting temperature. Several different approaches have been developed to address this problem.

This thesis focuses on a new modification of friction stir welding, called Laser Assisted Friction Stir Welding, a process developed in the last decade. This process uses laser energy to preheat the work piece at a localized area ahead of the rotating tool, thus softening a volume of the work piece ahead of the tool. The work piece is then joined by the rotating tool as in conventional FSW. The amount of heat generated during welding determines the quality of the weld. Hence understanding the temperature distribution is necessary in determining the optimum process parameters for the welding process. In this thesis, a three dimensional model of laser assisted friction stir welding is developed, using FLUENT which is based on finite volume method, to obtain the temperature distribution in the work piece. The developed model can be used to better understand the process, predict the process performance and to determine optimal process parameters. A comparison with pure friction stir welding without laser assistance is also made to show its potential benefits. Parametric studies are designed to understand the effect of variation of certain process parameters such as feed rate, tool rotational speed and laser heat input on temperature distribution in the work piece. Finally, optimal combinations of friction stir welding and laser parameters are determined by a metaheuristic - Ant Colony Optimization.

1. Introduction

1.1 Background

Friction Stir Welding is a relatively new welding process which was developed at The Welding Institute (TWI), United Kingdom, in 1991. Extensive research has been carried out to better understand this process. Researchers have explored different aspects of this process namely, tool design, weld microstructure, mechanical properties of the weld and many more. As a result of these efforts, FSW has been implemented in various applications around the world [1].

The Friction Stir Welding tool consists of a shoulder and a pin. The basic concept of this process is that a rotating tool pin is slowly inserted into the work piece to be welded, until the tool shoulder touches the top surface of the work piece and hold it there for a while to soften the material with generated frictional heat. The tool is then traversed along the path of interest, thus welding the plasticized volume behind it. A schematic of FSW process is shown in Figure 1.1 below.

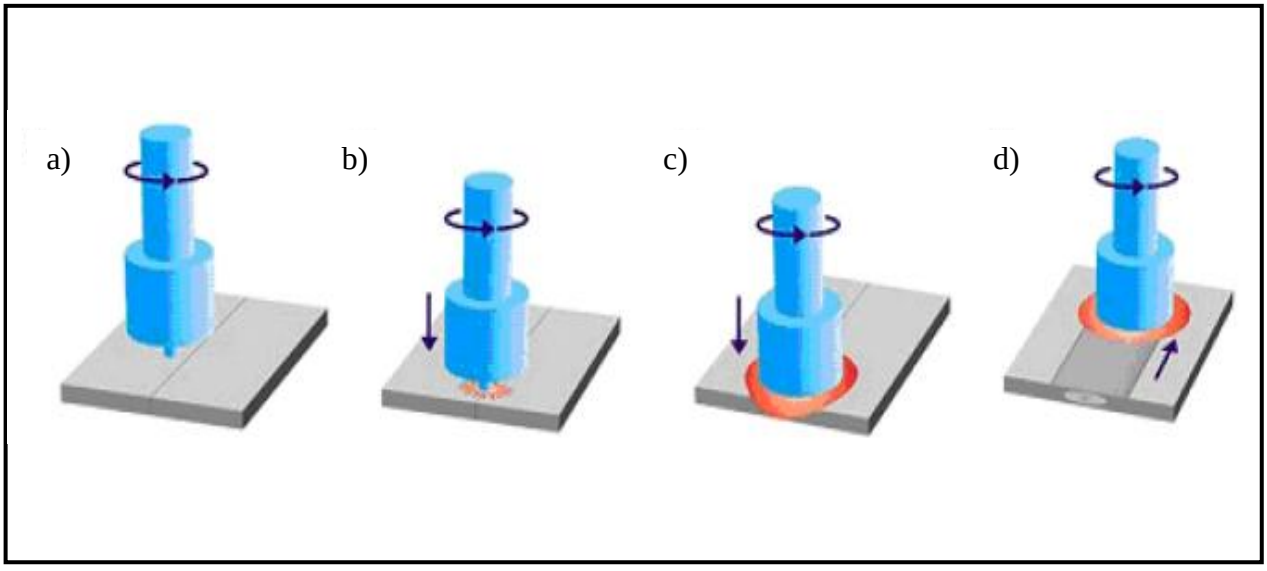

Figure 1.1 Schematic representation of FSW process: a) Rotating tool before plunging, b) Plunging stage, c) Tool shoulder touches the work piece surface producing frictional heat, d) Rotating tool traverses along the work piece

The work piece is placed on a backing plate and is clamped rigidly to the fixture to eliminate any degrees of freedom. Heat is produced due to shoulder surface friction with the top surface of the work piece, which softens the material to be welded. The tool shoulder is the primary means of generating heat during the process. It prevents expulsion of the material and guides the movement of the material during welding. The tool pin is normally $1/3^{rd}$ the diameter of the shoulder extending from the shoulder and rotates with a high speed of 1000's of rpm [2]. It is slowly plunged into the work piece until the shoulder surface touches the work piece. The pin then moves along the area to be welded on the work piece with a specified travel rate. Tool pin is the secondary means of heat generation. The pin of the rotating tool provides the stirring action to the materials of the two plates to be joined. As the tool travels along the path of interest, the weld cools, thereby joining the two plates together.

1.2 Advantages and Applications

FSW is a solid state process which takes place below the solidus temperature of the metal to be joined. Aluminum and Aluminum alloys can be easily welded by FSW and the process has been extended to various types of steels too [3]. FSW does not need a filler material as compared to conventional welding and is relatively easy to perform. Since no melting of the work piece material takes place, there are no work piece or tool material losses.

Amount of heat conducted into the work piece dictates the quality of the weld and the heat conducted back into the tool dictates the life of the tool. Insufficient heat produced from friction could lead to breakage of the tool pin since the material is not soft enough. One of the main process parameters in FSW is the heat flux. Heat flux should be high enough to keep the maximum temperature in the work piece to 80-90% of the melting temperature of the work piece material to avoid any welding defects [4].

Few other advantages of FSW process include:

- Fewer defects like porosity and voids due to absence of material melting
- Low distortion and residual stresses in welded zone
- Higher mechanical properties
- High joint strength, even in those alloys that are considered non-weldable by conventional techniques.

TWI patented FSW process in many industrial sectors throughout the world. Two of the very first industrial sectors which adopted friction stir welding for commercial purposes are shipbuilding and marine industries.

- Shipbuilding and marine industries: Some of the applications included panels for decks, helicopter landing platforms and aluminum extrusions.
- Automotive industry: In automotive sector, friction stir welding is used to replace fusion welding techniques. The process has been applied to the manufacture of tail light panels, automotive suspension arms etc.
- Aerospace industry: At present, aerospace industry is using production parts welded by Friction Stir Welding. Longitudinal butt welds in Al alloy fuel tanks for space vehicles have been friction stir welded and successfully used [7].
- Railway Industry: Commercial applications include building container bodies, railway tankers, etc.

1.3 Objective of This Study

Though FSW is a one of a kind welding process, it has several disadvantages. Since it is a solid state process, a great amount of tool wear takes place during the plunging stage as the work piece material is cold at this time. Weld speeds in FSW are slower which can lead to longer process

times. Since higher weld forces are required during this process, equipment used for FSW is massive and expensive. Moreover friction stir welding of high melting temperature materials such as steel and stainless steel are known to have welding tool limitations. Different approaches have been proposed to address these problems. The approach considered in this thesis is Laser Assisted Friction Stir Welding (LAFSW) which is a new modification of FSW developed in 2002. LAFSW is a combination of FSW and laser welding, with FSW being the dominant process and laser welding plays a supporting role. Figure 1.2 shows the schematic representation of laser assisted friction stir welding process.

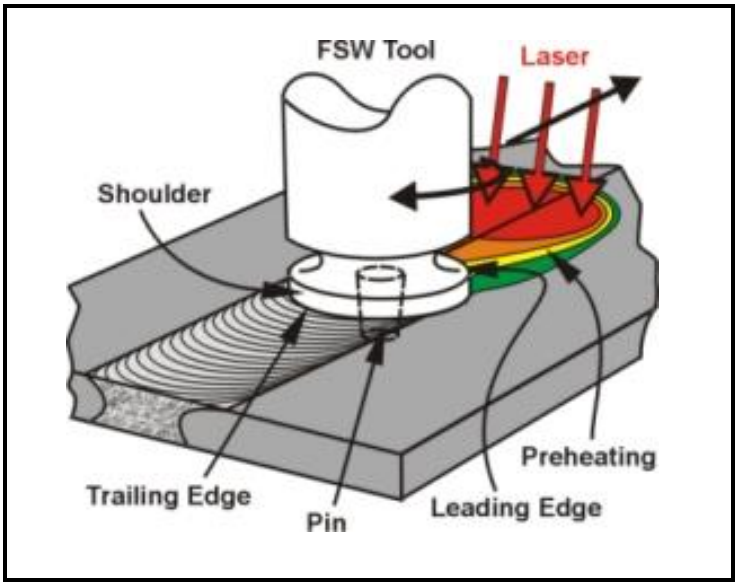

Figure 1.2 A schematic representation of laser assisted friction stir welding process

LAFSW was studied experimentally, to join AZ91D Mg alloy plates and other possible advantages of this method were also discussed [4]. The system combines a conventional commercial milling machine and Nd: YAG laser system. Laser power is used to preheat the work piece at a localized area ahead of the rotating probe, thus softening a volume of the work piece ahead of the probe. The work piece is then joined in the same way as in conventional FSW process. The high temperature ahead of the rotating tool softens the work piece and enables

joining without strong clamping fixtures. Less longitudinal force and downward force are required to move the tool ahead along the weld line, thus reducing tool wear. However, no model of laser assisted friction stir welding exists today. This study intends to fill in this gap.

Most of the FSW process knowledge is obtained through running experiments and then analyzing the results by comparing with the metallurgical specimens. Finite element modeling of FSW process, if done properly, would be an in-expensive way to examine the process which can help determine process parameters that require further experimental testing for verification and analysis. The process parameters of interest in Friction Stir Welding process have been tool feed rates and tool rotational speeds in many publications [5]. A lot of research has been carried out to investigate the effect of varying several process parameters on weld temperature history [6]. This thesis research focuses on the modeling and analysis of LAFSW process so that the developed model can be used to better understand the process, to predict the process performance and to determine the optimal process parameters. More specifically, the main objectives of this thesis are (i) to develop and validate a three-dimensional thermal model of laser assisted friction stir welding, (ii) to investigate the effects of varying process parameters on weld temperature history using the developed model, and (iii) to determine the optimal process parameters. A comparison with pure friction stir welding without laser assistance is also made to show its potential benefits.

2. Literature Review

2.1 On Modeling of Friction Stir Welding Process

Friction Stir welding was invented in 1990's and initial research included primarily experimental investigations of the process. Very few publications dealt with computational modeling and earlier models were restricted to heat transfer models only, as the process was relatively new. Feng and Gould published a heat flow model of friction stir welding, in which they considered heat generated at the tool shoulder only and studied how the heat is conducted into the plate [7]. In their model, heat input was a function of process parameters including tool rpm and force on the tool, and was applied as heat flux on top of the work piece with radius equal to that of the tool shoulder.

One of the first numerical models for FSW was produced by Chao and Qi [2]. In their paper, a transient three-dimensional thermo-mechanical model was produced. A constant heat flux input from the tool shoulder-work piece interface was assumed. The derived equation used for heat flux in their analysis is given by equation (1),

$$q(r) = \frac{3Qr}{2\pi r_0^3} \qquad \text{where } r \le r_0 \tag{1}$$

where *q(r)* is the rate of heat flux, r_0 is the tool shoulder radius, and *Q* is the heat input as a function of various process parameters as shown in equation (2).

$$Q = \frac{\pi\omega\mu F(r_0^2 + r_0 r_i + r_i^2)}{45(r_0 + r_i)} \tag{2}$$

The total heat input and heat transfer coefficient were calculated by fitting the measured data with the analytical model by a trial and error procedure. These temperatures were used as input for the mechanical model. Since the quality of the weld depends on the heat distributed in the work piece, it was believed that the heat flux should be high enough to keep the maximum

temperature in the work piece around 80% to 90% of the melting temperature of work piece material, so that weld defects are avoided [2]. Chao, Y.J., Qi, X. and Tang, W. [8] studied the heat transfer of the FSW process in both the work piece and the tool. A heat transfer problem was formulated as a standard boundary value problem and is solved by using the inverse modeling approach, comparing calculated temperature data with measured ones. Heat transfer in the tool is studied as a steady state analysis and that in the work piece as transient analysis. Some of the assumptions in their paper were summarized as follows:

- The downward force is applied to the work piece, creating a uniform pressure between the tool shoulder and the work piece.
- Heat is generated solely from the work done by the frictional force.
- Heat input is linearly proportional to the distance from the center of the tool.

It was concluded in their study that only about 5 % of the heat generated flows to the tool and remaining 95% flows to the work piece.

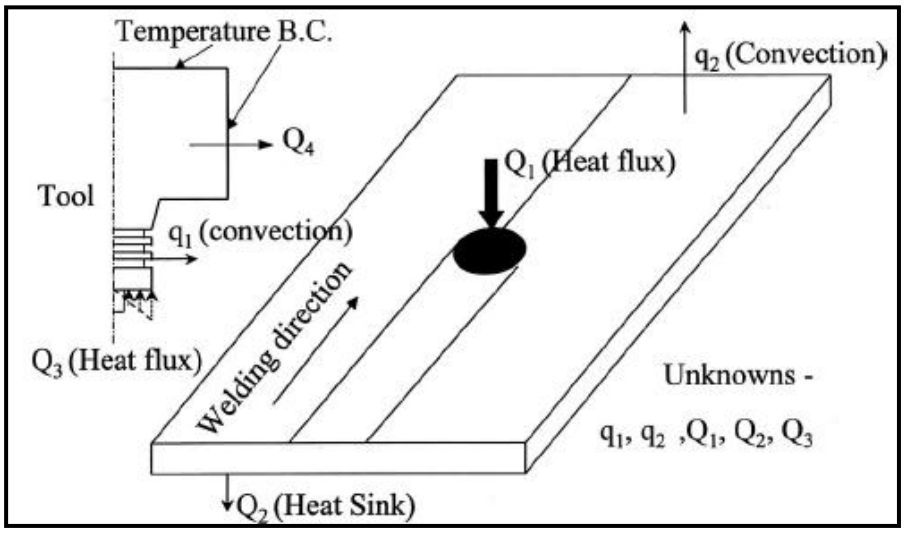

Figure 2.1 Schematic representation of boundary conditions used in [8]

Figure 2.1 shows the boundary conditions used in their model. Khandkar, M.Z.H., J.A. Khan, and A.P. Reynolds [9] proposed an input torque based model for FSW of aluminum alloys. In

their model, an approach was proposed for estimating heat input from moving and rotating welding tool. Heat input is correlated with experimentally measured torque data by assuming uniform shear stress at all the interfaces where the tool comes in contact with the work piece. The following equations are used to calculate torque at all the interfaces:

$$M_{shoulder} = \int_{r_i}^{r_0} (\tau r)(2\pi r)dr \tag{3}$$

where $M_{shoulder}$ is total torque at tool shoulder interface, r is the tool radii and τ is the torsional shear stress.

$$M_{pinbottom} = \int_{0}^{r_i} (\tau r)(2\pi r)dr \tag{4}$$

where $M_{pin\ bottom}$ is the torque at the pin bottom

$$M_{pinsurface} = (\tau r_i)2\pi r_i h \tag{5}$$

where $M_{pin\ surface}$ is torque at the pin surface. The total torque, M_{tot}, which is the sum of the above three components, was related to input power by equation (6),

$$P_{avg} = M_{tot}\omega \tag{6}$$

where ω is the tool rotational speed. The moving heat flux was calculated by equation (7),

$$q(r) = \frac{P_{avg} r}{\frac{2}{3}\pi r_0^3 + 2\pi r_i^2 h} \tag{7}$$

where r_0 is the shoulder radius, r_i is the pin radius and h is the pin length.

Reynolds, A.P., Tang, W., Khandkar, Z., Khan, J.A. and Lindner, K. [5] carried out a parametric study to explain the relationships between weld parameters, hardness distribution and temperature history in Al 7050 friction stir welds. Welds were made at different speeds using three different ratios of welding speed to tool rotation rate, called weld pitch. Welds were

performed under z-axis i.e. downward force control. Their results indicate that peak temperatures in the weld depend on both rotational speed and traverse speed of the tool. All the above authors incorporated heat flux as a moving heat source.

Song and Kovacevic [10] developed a three-dimensional moving co-ordinate heat transfer model for friction stir welding, in which heat input from the tool shoulder as well as the tool pin was considered. In their paper, tool pin penetration and pulling up condition were included in the finite element model. The work piece surfaces exposed to air have free convection and boundary condition at the tool shoulder-work piece interface and tool pin-work piece interface is a Neumann boundary condition. A convective boundary condition is applied at the face where the work piece touches the backing plate. Moreover, effects of preheating the work piece during FSW have also been discussed in their paper and they concluded that preheat is essential to increase the temperature of the work piece ahead of the FSW tool for protecting the tool from being worn out.

Studies have shown that the greatest amount of tool wear occurs during the tool pin plunging stage because the material is cold and high weld forces are required at this stage [11]. Therefore some methods like preheating the plunge area, drilling a partial penetration hole in the plunge area etc have been tried to minimize the effects of tool wear in friction stir welding as well as in many other processes. Such preheating methods will now be discussed in the next section of literature review.

2.2 On Laser Assisted Processing

Heat source obtained by means of laser energy is one of the most studied preheating methods. Effects of preheating are not only studied in FSW but also in various applications like arc welding, machining, deep drawing etc. Rozzi, J.C., Pfefferkorn, F.E., Incropera, F.P. and Shin,

Y.C. [12] developed a transient three dimensional model of Laser Assisted Machining of Silicon Nitride to examine the effects of laser preheating. Laser assisted machining provides an alternative machining process, for difficult to machine materials like structural ceramics, which can have higher material removal rates as well as improved control of material properties [12]. In their model, the work piece is locally heated by an intense laser source prior to material removal. Experiments were performed to determine the thermal response of a rotating work piece undergoing heating by a translating CO_2 laser and material removal by a cutting tool. Similarly, laser assisted micro end milling was studied by Jeon, Y. and Pfefferkorn, F. [13], in which they examined the effect of laser preheating on micro-end milling of Al 6061-T6 aluminum alloy and 1018 steel. The purpose of their study was to enable a significant increase in performance and productivity of the process which required higher spindle speeds and increased chip loads. Results in their study indicate that chip load can be significantly decreased and productivity can be significantly increased by local preheating of the work piece.

A mathematical analysis of laser assisted deep drawing process was carried out by Schuöcker [14]. In deep drawing, laser beams weaken the material near the drawing edge, where the material is bent. Due to the weakening of material edges, reduction in drawing forces can be obtained allowing processing of materials which are difficult to draw. Figure 2.2 shows schematic representation of the process. In figure 2.2, r_a is the unperformed work piece radius, r_i is the distance at which laser heating takes place, r_0 is the radius of the drawing edge and r_1 is the momentary radius during drawing process. It is proved in their study that drawing force reductions up to 50 % can be obtained due to laser assistance.

Preheating of work piece was not restricted to laser preheating. Other means of locally increasing the work piece temperature were also studied by some of the authors like Long and Khanna [11].

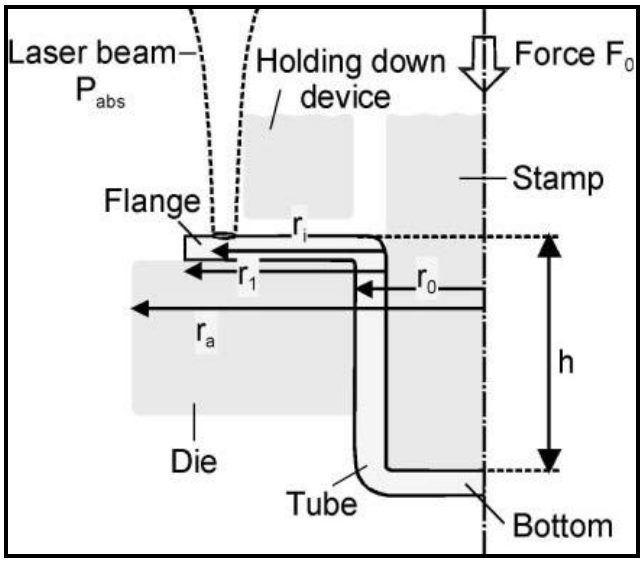

Figure 2.2 Schematic representation of laser assisted deep drawing process

In their paper, a new friction stir welding process, called electrically enhanced friction stir welding process, was developed to reduce the tool wear and to increase the welding speed. In this method, electric current passes through the work piece, in the welding region only, as the tool touches the work piece surface. This localized heating softens the material locally at the tool-work piece interface, thus reducing the plunge force on the FSW tool. Three kinds of heat sources were considered in that study and the total heat source is represented by equation:

$$q_0 = q_{0F} + q_{0P} + q_{0R} \tag{8}$$

where q_{0F} = frictional heat, q_{0P} = plastic work heat and q_{0R} = electrical resistance heat. In their paper, frictional heat is the main heat source in the upper part of the work piece, which is calculated as per equation (9),

$$q_{0F} = \frac{4\pi^2 \mu PNR^3}{3} \tag{9}$$

where μ = co-efficient of friction, P = pressure, N = tool rotational speed and R = tool shoulder surface radius. In their model, they assumed 60% of the heat input is from the tool shoulder

while 40% is by plastic work done due to stirring of tool pin. The heat source due to electrical resistance is calculated from the electric current heat generation according to equation (10),

$$q_{0R} = I^2 Rt \tag{10}$$

where I = current, R = electrical resistance and t = time for which current is passed.

Another method to overcome the drawbacks of FSW, was proposed by Kohn G., Greenberg Y., Makover I., and Munitz A. [4] known as Laser Assisted friction stir welding. This method was a combination of laser welding and friction stir welding, with laser welding supporting the FSW process for pre-heating purposes. The equipment for this method consisted of conventional vertical milling machine combined with multimode Nd:YAG laser system with a wavelength of 1064 nm. The work piece which was made up of Mg AZ91 alloy, was clamped to the milling machine table and laser energy was transmitted to the welding table by means of a 5m long optical fibre. The laser beam was defocused to form a 1 cm light spot ahead of the rotating probe. Microstructural specimens of the work piece were analyzed and it was concluded that resistance to the penetration, and to the forward motion of welding tool was negligible. Recently M. Merklein and Giera [15] carried out an experimental study of laser assisted friction stir welding of steel and aluminum sheets to increase weld feed and to reduce wear at the tool. In their paper, a parametric study was performed in order to detemine process parameters guarantying best mechanical properties of the welded parts. These publications as reviewed above are representatives of the current available open literature related to FSW and Laser assisted Friction Stir Welding.

2.3 On Process Optimization

There have been a lot of efforts to understand the effect of process parameters on weld temperature distribution, material flow, micro structural formation and mechanical properties of

the welded joint. In order to study the effects of process parameters like tool rotational speed, axial force and traverse speed, many researchers relied on empirical and experimental data for process optimization.

Conventional parametric design of experimental approach, being time consuming, some researchers like A.K Laxminarayanan and V. Balasubramaniyan [28] used Taguchi statistical technique to identify significant factors by conducting relatively less number of experiments. They adopted Taguchi L9 method to analyze the effect of rotational speed, traverse speed and axial force on tensile strength of FSW joints of RDE-40 aluminum alloy. Trial experiments were carried out to determine the range of process parameters for the FSW process. L9 orthogonal array design was selected for conducting experiments depending upon the number of parameters and number of levels of parameters of interest. Analysis of Variance (ANOVA) was performed by the authors to identify the process parameters which are statistically significant. From the experiments it was concluded that tool rotational speed has 41% contribution, traverse speed has 33% contribution and axial force has 21% contribution to tensile strength of welded joints.

Similarly, J.H Record, J.L Covington, T.W Nelson, C.D Sorensen, and B.W Webb [16] performed a 16-run factorial experiment to analyze the effects of nine FSW parameters on measured process outputs. Table 2.1 represents the process inputs selected for their study. Process parameter levels were chosen from within a known operational window that gave satisfactory welds. There were eight responses chosen for this analysis and significant factors were identified by means of Pareto Charts.

From their statistical experimentation, it was concluded that:

- Spindle speed, feed rate and plunge depth are the most significant factors of the FSW process.

- Z-force is most affected by the plunge depth; feed rate and weld location had secondary effects.
- X-force is most affected by feed rate, pin length and spindle speed.
- Shoulder temperature is most affected by spindle speed.

Table 2.1 Process inputs selected for factorial experiment [16]

Factor	Unit	Description
Spindle speed	rev/min	Revolutions per minute of FSW tool
Feed rate	mm/min	Speed of tool advancing through workpiece
Plunge depth	mm	Total distance tool is plunged (pin length + factor value)
Pin length	mm	Distance between outer edge of shoulder and tip of pin along tool axis
Weld cooling	n/a	Coolant circulation in cooling plate during weld
X start distance	mm	Location of plunge relative to edge of workpiece in X-direction
Weld location	n/a	Location of weld relative to edge of workpiece in Y-direction
Preweld cooling	Celsius	Amount of cooling before each weld, measured as the difference between the inlet and outlet temperatures of the cooling plate
Dwell time	seconds	Time between plunge sequence and weld traverse sequence

In case of experimental approach, trial and error methods to obtain optimal process parameters incurr considerable time and cost. The field of metaheuristics for the application to complex optimization problems is a rapidly growing field of research [17]. There are few publications studying the use of metaheuristics in various process optimizations and some of them are mentioned in this review. Kim D., Rhee S. and Park H. [18] presented a systematic approach to optimize welding process parameters by making use of Genetic Algortihm. In their study, the objective was to obtain desired weld geometry and the objective function used was as shown in equation (11),

$$J = (H_d - H)^2 + (W_d - W)^2 + (P_d - P)^2 \qquad (11)$$

where H_d, W_d and P_d are desirable bead height, bead width, and penetration, respectively, whereas H, W and P are bead height, bead width and penetration obtained from the experiment. Here, the objective was minimized to obtain desired bead geometry. This relationship between the input and ouput parameters was obtained by means of surface response methodology. Tarng, Y.S., Tsai, H.L. and Yeh, S.S.[19] used simulated annealing algorithm for searching process parameters with an optimal weld pool geometry. The objective function defined in their study was as per equation (12),

$$obj = w_1 FD + w_2 BH + w_3 BW \tag{12}$$

where, w_1,w_2,w_3 are the weights for the normalized front depth (FD), normalized back height (BH) and normalized back width (BW) of the weld respectively. This relationship between the welding process parameters and features on weld pool geometry was obtained by means of a neural network. Similarly, Sathiya P., Aravindan S., Haq A.N., and Panneerselvam K. [20] established a relationship between input and output variables of FSW process through artificial neural network (ANN). ANN is suitably integrated with the simulated annealing algorithm in order to find the optimal process parameters. These publications as reviewed above are representatives of the current available open literature related to the use of metaheuristics in welding process optimization.

3. Methodology Overview

To achieve the objective set forth for this thesis research, a methodology is developed. The first step is to develop a computational thermal model for laser assisted friction stir welding. It is chosen to develop the laser assisted part and add it to an existing friction stir welding model, which is also reproduced in this research. The friction stir welding model chosen for this task is the heat transfer model of Chao, Qi and Tang [8]. Hence, our first task is to replicate their model using the same process conditions as given in their paper, using Finite Volume Method software package FLUENT. The geometric model was developed independently in standard modeling software package, ICEM-CFD. The developed grid was then imported into the FLUENT solver for executing the solution. In order to validate the replicated model, the output of the model was then correlated with the published experimental data from the papers. The temperature distribution through the work piece was observed by means of the temperature contour plots and time-temperature graphs.

Once verified, the replicated model of friction stir welding was then modified to incorporate laser pre-heating. The next step is to test the feasibility for welding high melting temperature materials such as steel work pieces. The friction stir welding model chosen for this task is the heat transfer model of Zhu X.K. and Y.J. Chao [21]. The third step of the methodology is to carry out a parametric study of the modeled process. Specifically, we are interested in exploring the fundamental physical relationships governing the FSW process. Parametric studies were performed to observe the followings:

1. Effect of adding a pre-heating source on the FSW tool.
2. Effect of variation of tool feed rates on the temperature distribution in the work piece.
3. Effect of variation of FSW heat input on the temperature distribution in the work piece.

In this study, a screening design of experiments (DOE) is chosen to identify the effect of various weld inputs on temperature distribution in the work piece. Finally, the input-output data obtained from the DOE is used to obtain regression models and the optimal combination of laser welding and friction stir welding parameters is determined by Ant Colony Optimization method.

4. Transient Thermal Models of FSW

4.1 Introduction to Fluent 6

For over twenty years, Fluent Inc, which is now a subsidiary of ANSYS Inc, has been a leader in the development of Computational Fluid Dynamics (CFD) software for simulating fluid flow and heat and mass transfer. Fluent is a general-purpose CFD code based on the finite volume method on a collocated grid. Here the domain is discretized into a finite set of control volumes or cells. Fluent provides mesh flexibility, solving the flow problems with unstructured meshes that can be generated about complex geometries with relative ease. Fluent is written in the C computer language and makes full use of the flexibility offered by the language. All functions required to complete a solution and display the results are accessible in Fluent through an interactive, menu driven interface. The geometry and grid creation is an independent activity and can be developed using various standard modeling software packages like ICEM-CFD and GAMBIT. Once the grid is imported into the Fluent, all remaining operations like defining material properties, setting boundary conditions, executing the solution etc. are carried out in the Solver.

4.2 Comparison of Experimental and Numerical Analysis

In experimental investigation, it is very difficult to obtain high quality temperature data during FSW process. Accurate placement of thermocouples for recording temperature is tedious. In addition, thermocouples near the tool tend to move during the process, because of the material flow accompanying the process [5]. These drawbacks are overcome by numerical simulation as one can obtain temperature data at any required point in the model. Computer simulation has various advantages over experimental investigation. Some of them are listed below,

- Lower cost by avoiding the usage of experimental equipments.

- Computational investigation can be performed with remarkable speed as against experimental investigation.
- Computer simulation can provide values of all the relevant variables such as temperature, velocity, pressure etc, throughout the domain of interest.

4.3 Model Development of Friction Stir Welding for Al2195-T8

Since the heat transfer to the tool is minimal as compared to heat transfer to the work piece [8], thermal analysis of tool is not considered in this thesis. The first step in model development is building the model using ANSYS ICEM-CFD software package, which provides sophisticated geometric acquisition, mesh generation, wide variety of solver outputs and post-processing.

4.3.1 Geometry and Mesh Development

The only component of the model is the work piece. Due to the symmetry of the work piece, half model is used for the finite volume analysis as both halves are mirror images of each other. The work piece has dimensions of 610 mm*102 mm*8.1 mm as shown in figure 4.1.

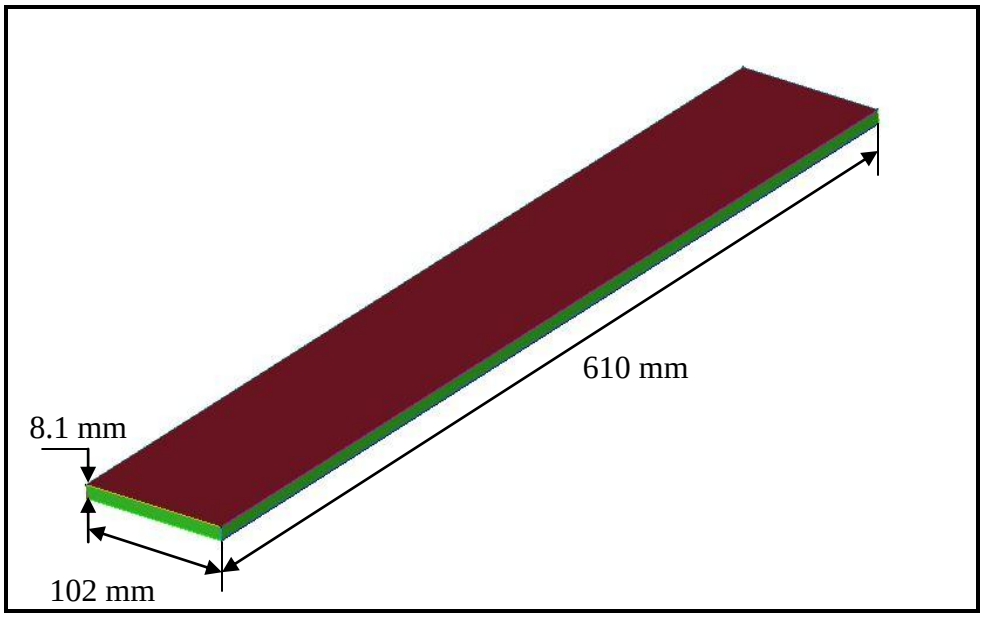

Figure 4.1 Isometric view of the work piece

Clamps on the top of the work piece have not been included in the model. As only heat transfer process is analyzed, clamping forces on the work piece can be neglected as they are at a sufficient distance from the tool. For grid formation, the work piece is divided into 200 parts along the length i.e. the X axis direction, 30 divisions along the width i.e. the Y direction and 10 divisions along the thickness i.e. the Z direction. Thus there are 62310 cells in the analysis. A time step of 3 seconds is used in the transient calculation. Figure 4.2 shows the mesh created by ANSYS ICEM-CFD. The model is a transient state model with moving heat source.

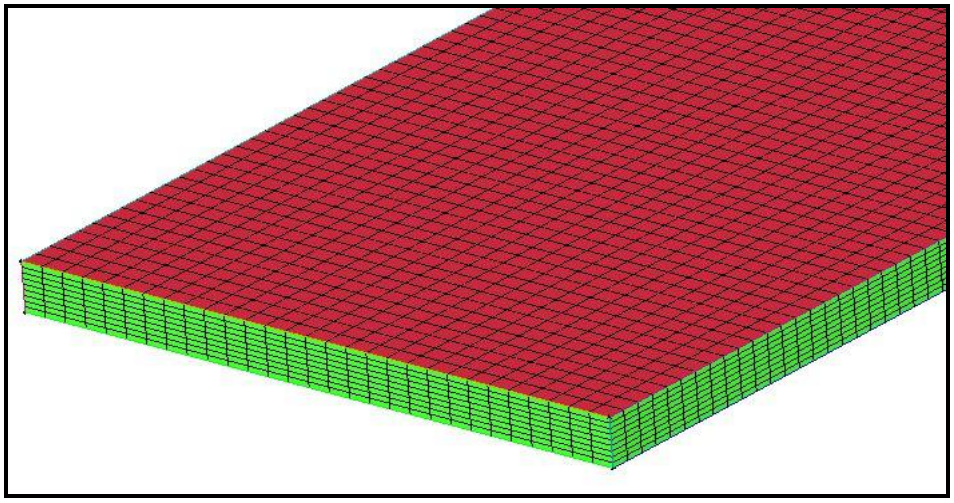

Figure 4.2 Isometric view showing meshed work piece

4.3.2 Material Properties

Once the modeling and meshing has been done, the grid is imported into Fluent. The next step of model development will be defining the material properties. Fluent-3-dimensional single precision solver is used for this analysis. Depending upon the application, material properties can be linear or non-linear. Linear properties are constant or temperature-dependent properties. Non-linear properties are tabular data such as creep data, plasticity data etc. The material selected for the present study is aluminum alloy Al 2195-T8. It is a solution heat treated, cold worked and artificially aged aluminum alloy.

Since our model is a transient thermal model, isotropic temperature dependent material properties are used for the analysis as given in table 4.1 below:

Table 4.1 Material properties of aluminum alloy Al 2195-T8

Temperature	°C	0	50	100	150	200	250	300
Thermal Conductivity	W/m °C	87	100	108	120	130	140	145
Heat Capacity	J/Kg °C	835	910	945	1000	1050	1085	1100

4.3.3 Boundary Conditions

Boundary conditions used for this model are based on data collected from several papers and thesis previously published [2, 8]. In Fluent, boundary conditions are associated with zones and not with individual cells or faces. The type of boundary condition selected is wall boundary condition according to Eq. (13), which is set for all the zones of the model. Since convective heat losses occur across all free surfaces, a convection co-efficient of 30 W/m^2 °C was applied to the top and side surfaces of the work piece.

$$-k\frac{\partial T}{\partial n} = h_{\infty}(T - T_{\infty}) \tag{13}$$

In equation (13), n represents the direction co-ordinate, h_{∞} is the ambient convection coefficient, k is the thermal conductivity of the work piece material, and T_{∞} is the ambient temperature. Since the contact condition between the bottom surface of the work piece and the backing plate is not known, a high heat transfer co-efficient was assumed off the bottom face of the work piece [2, 6, and 8]. Researchers have come to this assumption due to the fact that the exact contact resistance between the backing plate and bottom surface of the work piece is difficult to quantify. Due to complexity in accounting for the conductive heat loss through the bottom surface, a convection coefficient value of h = 350 W/m^2 °C, estimated by trial and error based on measured temperatures in [8], was applied to the bottom surface of the work piece in Eq. (14).

$$-k\frac{\partial T}{\partial z} = h(T - T_{\infty}) \tag{14}$$

The boundary condition at the tool-work piece interface is calculated from frictional heat. Since the temperature at the top surface of the work piece changes with respect to time, constant boundary conditions cannot be defined at the top surface. Such non-uniform boundary conditions are defined as profile functions instead of constant values.

Thus a User-Defined Function (UDF) has to be written, as given in Appendix A, in order to apply transient boundary condition on top surface of the work piece. UDF which is written in C programming language can be dynamically linked with the Fluent solver. Figure 4.3 shows the user interface for applying boundary condition to the top surface of the work piece.

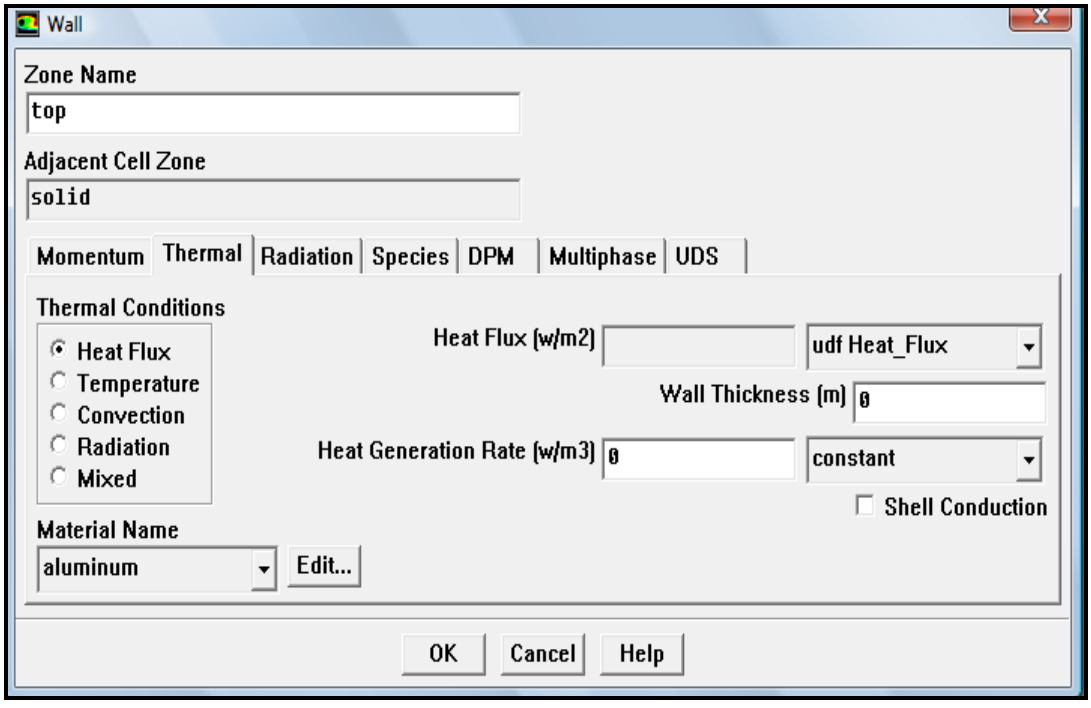

Figure 4.3 User interface for applying boundary condition to top surface of the work piece

Insulated boundary condition, where $\frac{\partial T}{\partial n} = 0$, is present along the mirror axis, i.e. interface between the two halves of the model. Since there is small heat loss to the tool, thermal analysis

of tool is not considered in this thesis. Also, as the difference in process temperatures and ambient temperature is relatively low, the percentage of heat loss due to radiation can be neglected [2].

4.3.4 Heat Flux Calculation

There are two heat sources involved in FSW which are generated by the friction at the interface between tool shoulder and work piece and plastic deformation of the welding material at the vicinity of rotating pin [2]. Heat produced due to plastic deformation is difficult to quantify and is significantly low [2], hence neglected in this study. Therefore, in this model heat generated by friction between tool shoulder and work piece is considered. In order to simplify the model, it was assumed that all the frictional heat produced is converted into heat and applied as circular heat flux on the top surface of the work piece. The rate of heat input to the work piece is calculated by the equation assumed by Chao, Y.J., Qi, X. and Tang, W. in [2, 8], which is as follows,

$$q(r) = \frac{3Qr}{2\pi(r_0^3 - r_i^3)} \qquad \text{for } r_0 \le r \le r_i \qquad (15)$$

In equation (15), Q (Watt) is the total heat input to the model, r_0 is the radius of the tool shoulder and r_i is the radius of the tool pin. The total heat input to the work piece is a function of several process parameters [2] and is calculated by equation (16),

$$Q = \frac{\pi\omega\mu F(r_0^2 + r_0 r_i + r_i^2)}{45(r_0 + r_i)} \qquad (16)$$

The heat input is assumed to be linearly proportional to the distance from the center of the tool which was derived from the assumptions, (a) the downward force applied to the work piece creates pressure between the tool shoulder and the work piece such that highest pressure will be

at the edge of the tool, and (b) the heat is generated from the work done by the friction force [2]. In this study, radius of the pin, r_i is assumed as zero. The tool shoulder diameter used in the study is 25.4 mm similar to Chao, Y.J., Qi, X. and Tang, W. in [8]. Calculating heat input is difficult as it involves many process parameters. Thus reverse engineering technique was used in [2] to find the total heat input from the resulting thermal profile. In Chao, Y.J., Qi, X. and Tang, W. [2], maximum temperature reached is assumed to calculate heat required to attain this temperature. For the verification of the model, heat input to the work piece was assumed to be 1740 Watt. The heat flux was translated along the length of the work piece with speed equal to the feed rate assumed as 2.33 mm/s.

User-defined functions are useful to customize the FLUENT code to fit particular modeling needs. Since transient boundary conditions cannot be defined by the FLUENT user-interface, a UDF is written to apply heat flux at the top surface of the work piece. Heat flux is defined as a custom boundary profile that varies as a function of spatial co-ordinates and time. The UDF is complied at the runtime by an in-built complier/interpreter in FLUENT. Once the UDF is interpreted, the function is available in the graphical interface of FLUENT. This UDF is called at every time step. In this user-defined function, weld center is calculated depending upon the current time. The UDF loops over all the cell faces on the top surface. Inside this loop, the distance between each cell face center and the current weld position is calculated. If this distance is less than or equal to the radius of the welding tool, heat flux shown by equation (15), is applied to that cell face, else convection is applied.

4.4 Model Development of Friction Stir Welding for 304L Stainless Steel

Following the same procedure used in Section 4.3, FSW of material 304L stainless steel is modeled, simulated and compared with the experimental results of X.K Zhu and Y. J Chao [21].

4.4.1 Geometry and Mesh Development for 304L Stainless Steel Work Piece

The method of creating geometry of the work piece and grid formation is similar to geometry and grid formation for aluminum alloy work piece as explained in section 4.3.1. In this study, the work piece has dimensions of 304.8 mm * 101.6 mm * 3.18 mm. For grid formation, the work piece is divided into 100 parts along the length i.e. the X axis direction, 30 divisions along the width i.e. the Y direction and 10 divisions along the thickness i.e. the Z direction. Thus there are 28179 cells in the analysis. A time step of 3 seconds is used in the transient calculation.

4.4.2 Material Properties for 304L Stainless Steel

Once the modeling and meshing has been done, the grid is imported into Fluent. Similar to section 4.3.2, our model being a transient thermal model, isotropic temperature dependent material properties are used for the analysis. The material selected for this study is 304L stainless steel which has a higher chromium and lower carbon content. The temperature dependent material properties are shown in table 4.2.

Table 4.2 Material properties of 304L stainless steel with respect to temperature

Temperature (^{o} C)	Thermal Conductivity (W/m^o C)	Specific Heat (J/Kg ^{o}C)
0	16	500
200	19	540
400	21	560
600	24	590
800	29	600
1000	30	610

4.4.3 Boundary Conditions for 304L Stainless Steel Work Piece

As explained in section 4.3.3, the type of boundary condition selected is wall boundary condition according to equation 13, which is set for all the zones of the model. To account for the heat losses to the ambient, convection and radiation boundary conditions are applied on all work piece surfaces except bottom surface.

The heat flux loss to the ambient is evaluated by equation (17),

$$q_s = h(T - T_0) + \varepsilon B(T^4 - T_0^4) \quad (17)$$

where T_0 is the room temperature, h = convection coefficient, ε = emissivity of the work piece surfaces, and B (= 5.67 X 10^{-12} W/cm^2 °C) is the Stefan-Boltzmann constant. A convection coefficient of 10 W/m^2 °C is applied on all the surfaces of the work piece except the bottom surface. On the bottom surface, a convection coefficient equal to 10 times the conventional convection coefficient of 304L stainless steel was applied to account for the heat flowing through the contact interface between the bottom surface of the work piece and the backing plate. Insulated boundary condition, where $\frac{\partial T}{\partial n} = 0$, is present along the mirror axis, i.e. interface between the two halves of the model.

4.4.4 Heat Flux Calculation

Heat produced due to plastic deformation is neglected in the work of X.K Zhu and Y. J Chao [21] and hence, not considered in this study. In this model, the heat generated by the friction between tool shoulder and work piece is applied as a circular heat flux on the top surface of the work piece. It is assumed in this work that heat flux is linearly distributed along the radial direction of the tool. The rate of heat input to the work piece is calculated by equation (15). In the current FSW process, since both FSW heat input and convection coefficient at the bottom surface of the work piece are unknown, an inverse analysis method is developed by X.K Zhu and Y. J Chao [21], to numerically solve the boundary value problem. For the verification of the model, heat input to the work piece was assumed to be 900 Watt. The heat flux was translated along the length of the work piece with speed equal to the feed rate assumed as 1.693 mm/s. The same User-Defined Function (UDF), as given in Appendix A, is used in this study in order to

apply transient boundary condition on top surface of the work piece. The UDF is hooked to the FLUENT solver in the same way as explained earlier in section 4.3.4.

5. Validation of Transient Thermal Models of Friction Stir Welding

In order to develop a useful LAFSW model, it was necessary to verify the FSW model with the results obtained from selected published papers. For this purpose, the developed three-dimensional thermal FSW model is verified with the experimental and numerical results obtained by Chao, Y.J., Qi, X. and Tang, W. [8]. The model used for validation had a work piece of material AA2195 with dimensions as 610 mm long, 102 mm wide, and height of 8.1 mm. The tool shoulder diameter was 25.4 mm and tool pin diameter was 10 mm. The rotational speed of the tool was 240 RPM and linear feed rate was 2. 36 mm/sec. Time dependent thermal properties of the work piece are shown in figure 5.1,

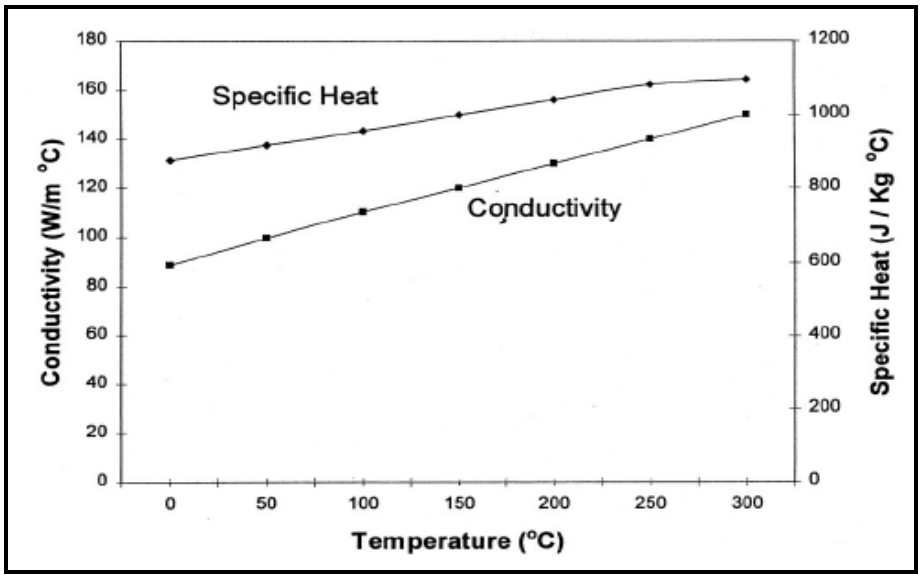

Figure 5.1 Material properties of AA 2195

A convective heat transfer coefficient of 30 W/m^2 °C was applied to the top and side surfaces of the work piece. A convection coefficient of 350 W/m^2 °C was applied to account for the heat flowing through the contact interface between the bottom surface of the work piece and the backing plate. The heat input to the system of Q = 1740 Watt was applied as circular heat flux to the top surface of the work piece. The tool started and stopped 20 mm away from both the edges

of the work piece and was traversed along the weld line. Experimental measurements were taken by Chao, Y.J., Qi, X. and Tang, W. through the use of thermocouples placed roughly at the center of the work piece at different locations and depths. Work piece temperature was measured at a distance of 305 mm, i.e. at the center of the work piece and 4 mm below the top surface, called the middle layer. Figure 5.2 shows the variation in temperature with respect to time at location (305, 5, 4) for both the results obtained by Chao, Y.J., Qi, X. and Tang, W. [8] and by the model developed in this study.

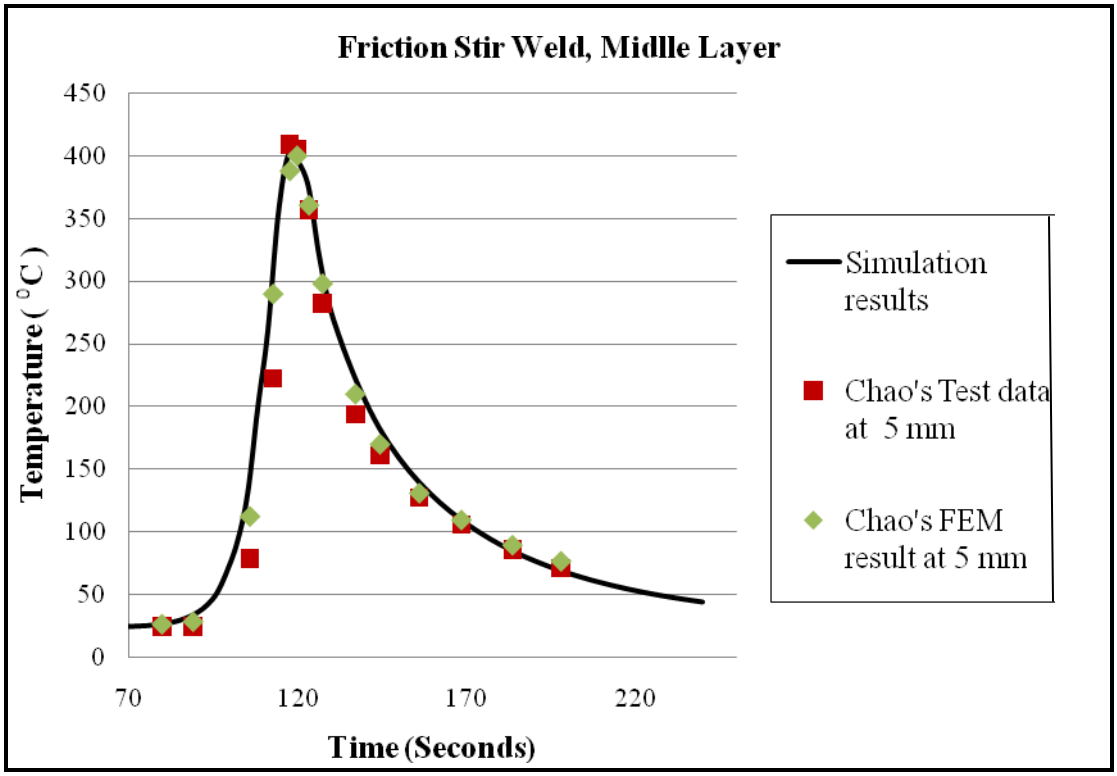

Figure 5.2 Comparison of simulation results and Chao's FEM and experimental results

In figure 5.2, the maximum temperature reached is 410 °C, which is very close to that in Chao's model [8]. Figure 5.3 shows the maximum temperatures obtained along the direction perpendicular to the weld line at X = 305 mm and 4 mm from the top surface. The highest temperature is observed at the weld center. The overall trend of the developed model is similar to

the model trend of Chao, Y.J., Qi, X. and Tang, W. [8], which is required for a valid verification. The results of the simulation are in good agreement with the experimental results, thus verifying the validity of the model developed in this thesis [10].

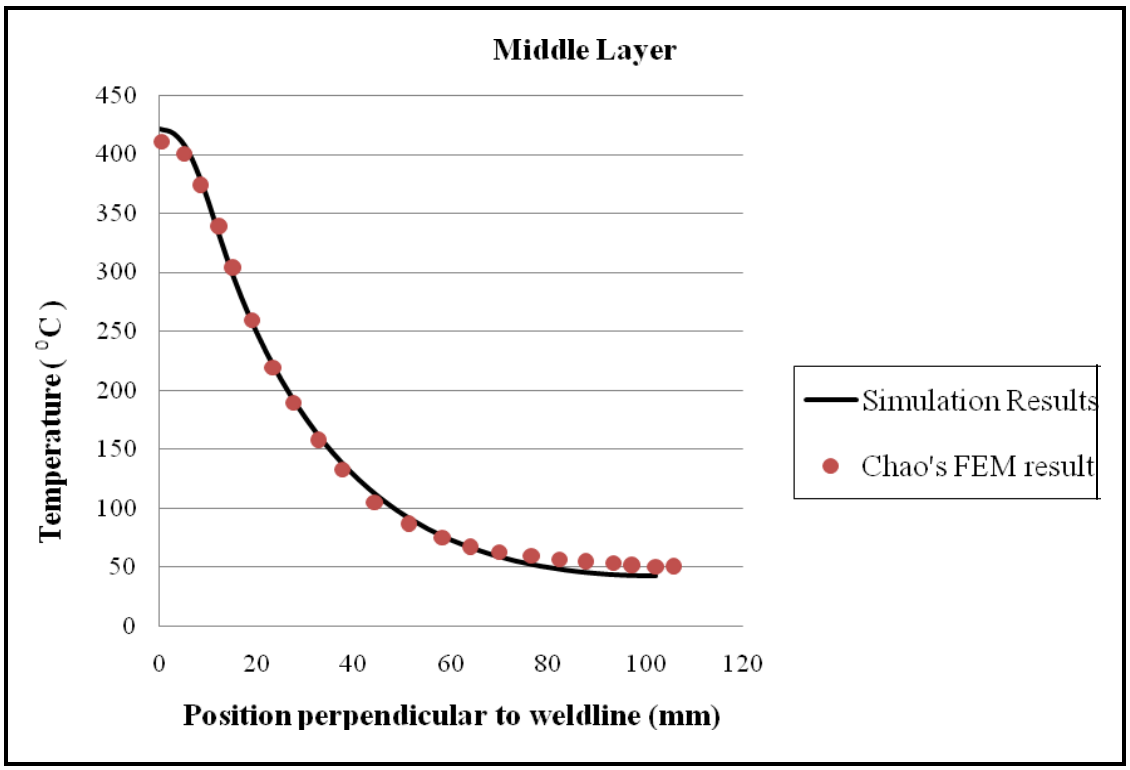

Figure 5.3 Comparison of temperature data perpendicular to the weld line

Similarly, friction stir welding of material 304L stainless steel is simulated and compared with the experimental results of X.K Zhu and Y. J Chao [21] .The model used for validation had a work piece with dimensions 304.8 mm × 203.2 mm × 3.18 mm and the tool rotational and translational speeds were 300 rpm and 1.693 mm/sec respectively. The tool shoulder diameter was 19.05 mm and tool pin diameter was 6.35 mm. A convection coefficient of 10 W/m^2 °C is applied on all the surfaces of the work piece except the bottom surface. On the bottom surface, a convection coefficient of 125 W/m^2 °C was applied. The heat input to the system was Q = 900 Watt and was applied as circular heat flux to the top surface of the work piece.

The tool starts 6.4 mm away from the edge of the work piece and stops after a translation of 279.4 mm along the weld line. Work piece temperature was measured on the top surface at a distance of 152.4 mm, i.e. at the center of the work piece. Figure 5.4 shows the variation in temperature with respect to time at location (X=152.4, Y=12.7 and Z=0) for the results obtained by X.K Zhu and Y. J Chao [21] and by the model developed in this study.

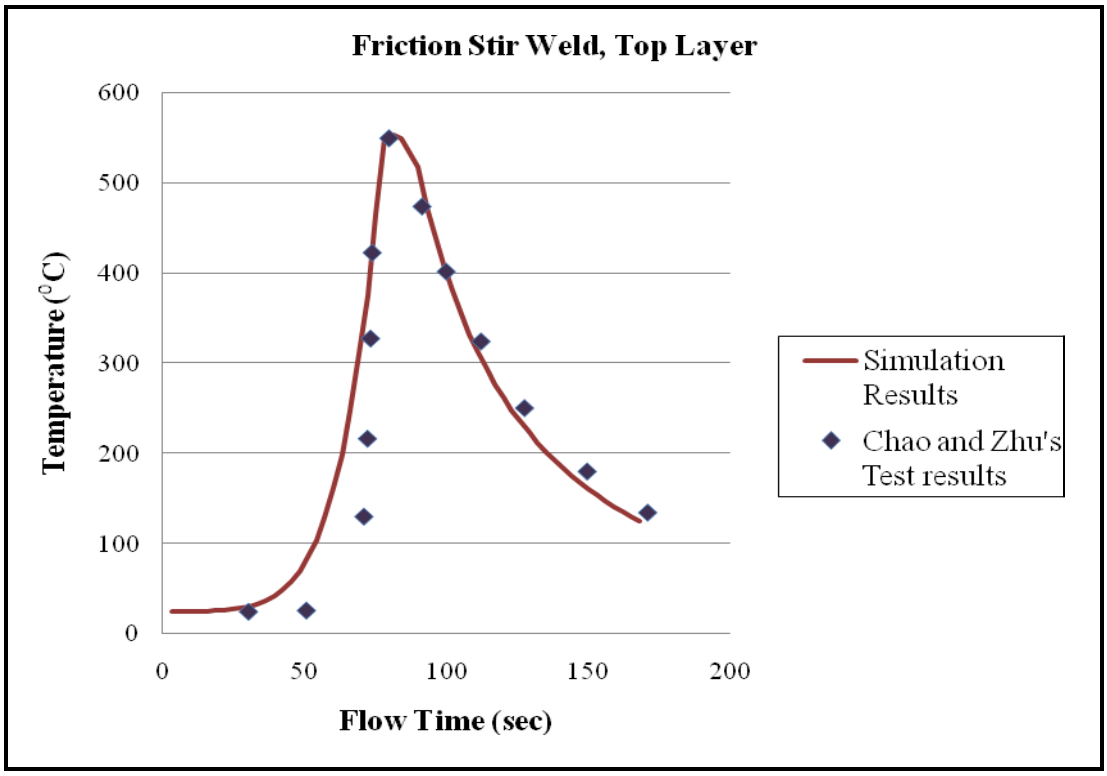

Figure 5.4 Comparison of simulation results and X.K Zhu and Y. J Chao's FEM and experimental results

The highest temperature is observed at the weld center. The overall trend of the developed model is similar to that of X.K Zhu and Y. J Chao [21], which is required for a valid verification. The results of the simulation are in good agreement with the experimental results, thus verifying the validity of the model developed in this thesis.

6. Parametric Study of FSW Process

6.1 Design of Experiments

In this study, the effects of various welding parameters on work piece temperature distribution were experimented using design of experiments and statistical design approach. Design of Experiments (DOE) is a statistical method used to study many variables simultaneously and quantify their effects on a given response relative to each other [16]. With the help of Design of Experiments, simultaneous study of effects that several factors have on a process can be studied. Such designs are efficient in terms of time and cost and also allows for the study of interactions between the factors.

The results obtained from the developed simulation in chapter 4, correlated well with the experimental results at various locations of the work piece. Using the friction stir welding model in chapter 4, a parametric study is designed to analyze the controllable parameters with respect to weld quality and FSW process productivity. The first step in this process is to identify the factors that would be varied. The parameters or control variables considered in this study are tool translational speed, friction stir welding tool heat input and tool shoulder diameter. The next step is to determine the levels of these factors. Parameter levels were chosen from within a known operational window obtained from various research papers [6,22, 23]. Table 6.1 shows the materials and the parameter levels used in this study. The final step in the parametric process is to perform the experiments and analyze the information. This thesis utilizes an 18-run screening DOE to analyze effects of 3 input parameters on selected output. The design consist of 3 independent variables namely feed rate (v), friction stir welding tool heat input (Q) and friction stir welding tool shoulder diameter (ϕ), as shown in table 6.1, and 1 dependent (response) variable, work piece temperature (T).

Table 6.1 Parameter levels selected for performing design of experiments

Materials	Design Factors	Low	Medium	High
Aluminum alloy-2195	Feed Rate (mm/sec)	1.5	2.33	4.2
	Heat Input (Watt)	1500	1760	1860
	FSW Tool diameter (mm)	19	-	25.4
304L Stainless Steel	Feed Rate (mm/sec)	0.55	1.69	2.55
	Heat Input (Watt)	1000	1200	1500
	FSW Tool diameter (mm)	15	-	19

The material properties and boundary conditions applied in the model for parametric design are the same as that applied by X.K Zhu and Y. J Chao [21] for stainless steel and Chao, Y.J., Qi, X. and Tang, W [8] for Al-2195-T8. The simulation is run 18 times in FLUENT as explained in chapter 4 and peak temperatures are recorded at a point in the aluminum alloy work piece which is located at X = 305 mm, Y = 5 mm, Z = 4 mm. Table B.1 in appendix B, depicts the factors and factor levels and the measured response in screening design for aluminum alloy work piece.

Similarly, the simulation is run 18 times in FLUENT for stainless steel and peak temperatures were recorded at a point in the work piece which is located at X = 152 mm, Y = 12.7 mm, Z = 0 mm. Table B.2 in appendix B, depicts the factors and factor levels and the measured response in screening design for stainless steel. It is important to note that any information about the analysis only applies for the range of parameters tested and for this experimental set up. This information may, or may not apply to other FSW conditions. Once the input-output data is obtained, to estimate temperature distribution for FSW process, regression models were formulated through multiple linear and non linear regression analyses.

6.2 Development of Models for Estimating the Temperature Distribution

6.2.1 Regression Analysis for FSW Model of Aluminum Alloy-2195

The extracted data obtained in table B.1 is analyzed in Minitab, statistical software capable of DOE analyses as well as regression analyses. Temperature in the work piece was selected as the

dependent variable and three independent variables were used to determine the regression equation. Before performing linear regression in Minitab, the correlation between dependent variables and independent variables was observed. Correlation quantifies the strength of linear relationship between two variables. From table C.1 in appendix C, tool feed rate has a correlation coefficient of -0.791 with work piece temperature. It indicates that when feed rate increases, work piece temperature tends to decrease. Since the p-value is less than the selected α-level (0.05), the results suggest linear relationship between feed rate and temperature. Correlation coefficient between FSW tool heat input and work piece temperature and between tool shoulder diameter and work piece temperature is low. Usually, the larger the correlation coefficient is, the larger the effect a variable will have. However, because the correlation coefficient depends only on linear relationship between the response and the variable, a more advanced regressor selection procedure is required.

To develop more reliable models, the variables were applied to a regression model and linear regression equation (18) was obtained from the analysis.

$$T = 334 + 0.2 * Q - 44.7 * v - 6.53 * \phi \qquad (18)$$

The complete regression analysis is included in Appendix D. The standardized regression coefficients are listed in table 6.2. These coefficients are useful in determining the significance of individual independent parameters. As it can be seen from this table, the linear effects of feed rate have the most significant influence on work piece temperature.

Table 6.2 Standardized regression coefficients for Al-2195 work piece temperature

Predictor	**Coefficient**	**SE Coefficient**	**T**	**P**
Constant	-0.000	0.05161	-0.0	1.000
Heat input	0.476	0.05310	9.27	0.000
Feed Rate	-0.7911	0.05310	-14.90	0.000
Tool ϕ	-0.3275	0.05310	-6.17	0.000

Since it could not be asserted that linear effects of all independent parameters influence the response variable, i.e. the work piece temperature, a regression model was formulated through multiple non linear regression analyses. The extracted data obtained in table B.1 in appendix B, was analyzed in DataFit version 9.0, a statistical software capable of data plotting as well as regression analyses. DataFit uses a set of pre-defined models for fitting data. Nonlinear regression, being an iterative process, initial values for each parameter, is picked by the software itself. It then adjusts the initial values to improve the model and best-fit parameter values are interpreted. The variables were applied to a set of non linear models and non linear regression equation which best fits the data was obtained as follows,

$$Y = \exp(0.0005012 * Q - 0.114 * v - 0.01637 * \phi + 5.82) \quad (19)$$

The complete non linear regression analysis is included in Appendix E.

6.2.2 Regression Analysis for FSW Model of 304L Stainless Steel

The extracted data obtained in table B.2 in appendix B, is analyzed in Minitab, and the correlation between dependent variables and independent variables was observed. From table C.2 in Appendix C, it can be seen that, FSW heat input has a correlation coefficient of 0.732 with work piece temperature. It indicates that when FSW tool heat input increases, work piece temperature tends to increase. Since the p-value is less than the selected α-level (0.05), the results suggest linear relationship between FSW heat input and temperature. Feed rate and tool shoulder diameter have lower correlation with the work piece temperature. Since it cannot be asserted that a linear relationship exists between the response and the variable, a more reliable model is required. Thus, to develop more reliable models, the variables were applied to a regression model and linear regression equation (20) was obtained from the analysis.

$$T = 149 - 96.1 * v + 0.424 * Q + 4.97 * \phi \quad (20)$$

The complete regression analysis is included in Appendix D. The standardized regression coefficients are listed in table 6.3.

Table 6.3 Standardized regression coefficients for 304L stainless steel work piece temperature

Predictor	Coefficient	SE Coefficient	T	P
Constant	0.00	0.03516	0.00	1.000
Feed Rate	-0.6619	0.03618	-18.24	0.000
Q	0.7324	0.03618	20.24	0.000
ϕ	0.0836	0.03618	2.31	0.036

As it can be seen from this table, the linear effects of heat input have the most significant influence on work piece temperature. It may be possible that there exists a strong non linear relationship between feed rate and work piece temperature or between laser heat input and work piece temperature. Since it could not be asserted that linear effects of all independent parameters influence the response variable, i.e. temperature, a regression analysis was formulated through multiple non linear regression analyses.

The extracted data obtained in table B.2 is analyzed in DataFit version 9.0. Since correlation between certain variables could not assert a linear relationship, the variables were applied to a set of non linear models and non linear regression equation was obtained as follows,

$$Y = \exp(-0.1586 * v + 0.000691 * Q + 0.00764 * \phi + 5.65) \qquad (21)$$

The complete non linear regression analysis for stainless steel is included in Appendix E.

6.3 Estimating Performance of Linear and Non Linear Regression Models for FSW Process on Temperature Distribution

The results in Appendix D and E show how accurately the linear and nonlinear models estimated the temperature in the work piece with respect to the change in tool feed rate, heat input and tool shoulder diameter. To find the optimal model which best fits the data, certain statistical terms such as adjusted coefficient of determination are used in this thesis.

Adjusted Coefficient of determination (R^2_{adj}) is a non-dimensional measure of how well a regression model describes the data and can be used to obtain the optimal regression model. Other statistical measures like, Durbin-Watson statistic and Akaike's Information Criterion (AIC) are used in this thesis, to study the adequacy of the outcome of the regression analysis. Durbin-Watson statistic, values of which are between 0 and 4, is used to determine autocorrelation of the residuals from the regression analysis. Autocorrelation of the residuals indicate that the model can be still improved and leads to biased estimates of statistical significance of the parameters. Durbin-Watson value towards 2 indicates non-autocorrelation; a value towards 4 indicates negative autocorrelation and a value close to 0 indicates positive correlation. Akaike's information criterion is a measure of the goodness of fit of an estimated statistical model and can be calculated by the following equation (22).

$$AIC = 2k + n*\left[\ln(2\pi SS_{res}/n) + 1\right] \quad (22)$$

A set of competing models can be ranked according to their AIC and the model with the lowest AIC is selected as the best fit model. Table 6.4 shows the regression statistics of the FSW process for Al -2195 alloy and 304L stainless steel.

Table 6.4 Regression statistics of the FSW process for Al -2195 alloy and 304L stainless steel

Process	**Regression Model**	R^2_{adj}	**Durbin-Watson statistic**	**Akaike's Information Criterion (AIC)**
FSW of Al -2195	Linear	0.952	2.92	131.53
	Non linear	0.978	2.82	117.29
FSW of 304L stainless steel	Linear	0.978	1.93	140.09
	Non linear	0.988	2.73	128.308

Referring to the Durbin-Watson significance tables, it is concluded that there is no autocorrelation of the residuals from any of the regression analysis. From table 6.4, it is seen that R^2_{adj} for non linear regression models is higher for both the materials, which indicates that the

non linear regression model as given by equations 19 and 21 fits the data better than the linear regression model given by equation 18 and 20 for both Al-2195 and 304L stainless steel. The lowest AIC statistic was observed for non linear regression models of both the materials, which indicate that non linear regression models given by equation 19 and 21 best fit the data given in Appendix B. Thus the best models for estimating the work piece temperature were the non linear regression models for both Al-2195 alloy and 304L stainless steel.

7. Determining Optimal FSW Parameters by Ant Colony Optimization

Ant colony optimization is a population based general search technique for the solution of different combinatorial problems which is inspired by the pheromone trail laying behavior of real ant colonies. When an ant finds a food source, it evaluates the quantity and the quality of the food and carries some of it back to the nest. During the return trip, the ant deposits a chemical pheromone trail on the ground. The quantity of pheromone deposited, which may depend on the quantity and quality of the food, will guide other ants to the food source. Indirect communication between the ants via pheromone trails enables them to find shortest paths between their nest and food sources. Modifications have been made to develop versions suitable for continuous function optimization. Our implementation follows the Ant Colony Optimization for continuous domain (ACO_R) algorithm proposed by Socha, K. and Dorigo, M. [24]. To handle constraints, the parameterless penalty method proposed by Deb. K. [25] is incorporated into ACO_R. The pseudo code of the implemented ant colony optimization algorithm, called ACO_R+, is given below.

Algorithm ACO_R+

Step 1: Initialize parameters, which include number of ants: *n*, maximum number of function evaluations: *maxnfe*, a parameter that controls intensification versus diversification: *q*, a positive parameter that has an effect similar to that of the pheromone evaporation rate:ξ, and the size of solution archive, *k*.

Step2: Randomly generate *k* solutions and evaluate them as the initial solutions in the archive. Initialize number of function evaluations, *nfe* = *k*.

Step 3: Rank the solutions in the archive to put feasible solutions ahead of infeasible solutions first, then rank feasible solutions in descending order of their objective values, and lastly rank infeasible solutions in descending order of constraint violation.

Step 4: Compute the weight of solution *l* in the archive, according to Eq. (7) in Socha, K. and Dorigo, M. which is denoted by equation (23) as follows:

$$\omega_l = \frac{1}{qk\sqrt{2\pi}} e^{\frac{-(l-1)^2}{2q^2k^2}} \tag{23}$$

where, *k* = length of solution archive.

Step 5: Compute the probability for choosing a solution in the archive, according to Eq. (8) in Socha, K. and Dorigo, M. The following equation (24) computes the probability of choosing *l*th solution in the archive:

$$p_l = \frac{\omega_l}{\sum_{r=1}^{k} \omega_r} \tag{24}$$

Step 6: **While *nfe* < *maxnfe***

For each ant

i. Choose a solution from the archive by roulette selection based on the probability computed in equation (24).

ii. Compute the standard deviation associated with the selected solution, σ_l, according to Eq. (9) in Socha, K. and Dorigo, M., which is denoted by equation (25) below.

$$\sigma_l^i = \xi \sum_{e=1}^{k} \left| S_e^i - S_l^i \right| / (k-1) \tag{25}$$

where *k* is the length of the solution archive.

iii. Construct a trial solution by updating the selected solution by $\pm\, rand \cdot \sigma_l$, with *rand* being a uniformly distributed random value $\in [0, 1]$.

iv. Repair the trial solution for any variable that is out of bound by either randomly generating one or setting it to the bound value.

v. Evaluate the trial solution and increment *nfe* by one.

vi. Update the archive if the trial solution is better than the worst in the archive.

End for

Step 7: Update the best solution

End while

Step 8: Output the result of optimal solution and its objective value

---

In summary, ACO_R+ differs from ACO_R mainly in the following areas. First of all the evaluation function has to compute not only objective value but also constraint violation. Secondly, one additional column has to be added to the solution archive to store constraint violation information. Thirdly, the ways that solutions are ranked and best solutions is selected have to be changed. Major parameters associated with the ACO_R+ algorithm include number of ants, *n*, maximum number of function evaluations, *maxnfe*, a parameter that controls intensification versus diversification, *q*, and a positive parameter that has an effect similar to that of the pheromone evaporation rate, ξ, the size of solution archive, *T*. For this study, they are fixed at 30, 150,000, 0.7, 0.7 and 15, respectively.

7.1 Formulation of Optimization Models

For any manufacturing process, it is desirable to achieve maximum throughput, good quality, and minimum cost. There is no exception for the friction stir welding process of concern in this research. Therefore, to determine the optimal process parameters we formulate the optimization models as follows:

Maximize Throughput

Minimize Cost

Subject to,

i) Good quality of the weld

ii) Bounds of process parameter values

In welding, throughput for some duration of time can be measured by the length of weld made that depends much on the welding speed used. Welds cannot be made without energy input. Given that equipment cost and labor cost are fixed, energy input is the dominant cost component. Since weld quality is the result of thermal history during welding, the weld quality constraint can be equated with a temperature constraint. Of course, the possible values of a process parameter are often limited to the range available in the system used to carry out the process. This range can be further reduced as knowledge in operating the system for a particular job is gained over time.

In this research, the two conflicting objectives are handled by combing them into one single objective function. The weights applied to each of the two objectives are assumed equal. To offset the magnitude difference between the two objectives, the objective with lower magnitude is multiplied by a constant α. Specifically, two optimization models to be solved by the ant colony optimization algorithm have the following form:

Minimize $H - \alpha S$

Subject To: $T_{LB} \leq T \leq T_{UB}$

$H_{LB} \leq H \leq H_{UB}$

$S_{LB} \leq S \leq S_{UB}$

$D_{LB} \leq D \leq D_{UB}$

where T is the temperature, H is the heat input, S is the feed rate, and D is the friction stir welding tool diameter. $_{LB}$ and $_{UB}$ stands for lower bound and upper bound. The two models differ

primarily on the equation for T: called Model 1 if linear equations (18) and (20) are used and Model 2 if non linear equations (19) and (21) are used instead, for easy reference later.

7.2 Optimization Results for FSW of Al-2195 T8 and 304L Stainless Steel

The ant colony optimization algorithm was applied to solve the optimization model formulated in the previous section for FSW of Al2195-T8 by setting α=500, T_{LB} = 450, T_{UB} = 475, H_{LB} = 1,500, H_{UB} = 1,860, D_{LB} = 19, and D_{UB} = 25.4. Due to the stochastic nature of the algorithm, a total of 30 runs were made to generate sufficient statistical data. The best, medium, and worst objective values and CPU time taken are recorded, along with the optimal solution. Table 7.1 summarizes the optimization results for FSW of Al-2195 T8, for both Model 1 and Model 2. The same optimization model can be solved by simple nonlinear programming (NP). The '*fmincon'* function available in Matlab was used to find a constrained minimum of a scalar function of several variables starting at an initial estimate. Table 7.1 also summarizes the optimization results obtained by 'fmincon' for FSW of Al-2195 T8, for both Model 1 and Model 2.

Table 7.1 Optimal solutions for FSW of Al2195-T8

		By NP		**By ACO**	
		Model 1	**Model 2**	**Model 1**	**Model 2**
Objective Value	Best	384.2729	404.059	384.2729	404.059
	Median	384.2729	404.059	384.2729	404.059
	Worst	384.2729	404.059	429.18	433.44
Best Solution	Heat Input	1860	1860	1860	1860
	Welding Speed	2.9514	2.911	2.9514	2.911
	Tool Diameter	19	19	19	19
CPU time	Best	0.0312	0.0468	19	18.33
	Median	0.0780	0.0936	22.18	23.30
	Worst	2.0904	2.3088	25.55	25.64
Number of runs found the best solution		30	30	26	27

Similarly, the optimization model formulated was solved by nonlinear programming as well as ant colony optimization for FSW of 304L stainless steel. For ant colony optimization, the upper

and lower bounds were set as: α=500, T_{LB} = 750, T_{UB} = 800, H_{LB} = 1000, H_{UB} = 1500, D_{LB} = 15, and D_{UB} = 19. A total of 30 runs were made to generate sufficient statistical data. The best, medium, and worst objective values and CPU time taken are recorded, along with the optimal solution. Table 7.2 summarizes the optimization results by non linear programming and ant colony optimization, for FSW of 304L Stainless Steel, for both Model 1 and Model 2.

Table 7.2 Optimal solutions for FSW of 304L stainless steel

		By NP		**By ACO**	
		Model 1	**Model 2**	**Model 1**	**Model 2**
Objective Value	Best	826.58	832.95	826.58	832.95
	Median	826.58	832.95	826.58	832.95
	Worst	826.58	832.95	826.594	937.16
Best Solution	Heat Input	1500	1500	1500	1500
	Welding Speed	1.346	1.334	1.346	1.334
	Tool Diameter	19	19	19	19
CPU time	Best	0.0156	0.0312	18.92	18.829
	Median	0.078	0.0936	19.76	20.13
	Worst	2.1996	2.1684	22.49	28.7
Number of runs found the best solution		30	30	29	29

It is observed that, the optimization models are simple enough to be solved by gradient based nonlinear programming procedure. On the other hand, Ant Colony Optimization can be useful to solve more complicated models such as non convex and non differentiable ones where gradient based methods would be ineffective. Thus in this section, optimal process parameters were determined for Friction Stir Welding process for both Aluminum Alloy-2195 T8 and 304L Stainless Steel.

8. Laser Assisted Friction Stir Welding Model

The validated friction stir welding model is subsequently modified to incorporate laser heat source. For showing potential benefits of laser assisted friction stir welding, Aluminum alloy-2195 is used as the work piece material. The values of power required from the laser should be such that it can raise temperature of the work piece to about 0.4 times the melting temperature of the work piece material [26]. Laser heat input is applied as a circular heat flux, ahead of the friction stir welding tool, with a radius of 5 mm and 800 Watt heat intensity. Gaussian heat flux equation is used, as in [27], to calculate the laser heat flux incident on the work piece which is given in equation (26),

$$q(r) = \frac{2Q}{\pi r_b^2} e^{\frac{-2r^2}{r_b^2}} \tag{26}$$

where Q is the laser power, r_b is the beam radius at the work piece top surface, and r is the radial distance from center of the laser beam. The laser heat source was assumed to have Gaussian distribution in the radial direction with maximum heat flux at the center. In this study, laser conduction welding model is considered and there is no keyhole formation. Laser conduction welding depends on the conductivity of the material being welded. Laser beam is focused on a specific area ahead of the friction stir welding tool, due to which heat is generated. The overall temperature in the domain remains below the melting point of the work piece material.

The UDF developed in chapter 4 needs to be modified, to incorporate laser heat source (Appendix A). Laser heat input is applied as a circular heat flux on the top surface of the work piece, which is computed by equation (26). It is defined as a custom boundary profile, similar to FSW heat flux, which varies as a function of spatial co-ordinates and time. Weld center for laser heat flux, is calculated depending upon the current time, similar to FSW heat flux described in

chapter 4. Both the heat sources are assumed to have the same linear velocity, i.e. 2.33 mm/sec. The distance between the center of friction stir welding tool and the point at which pre-heating laser source starts is fixed to 20 mm. The UDF loops over all the cell faces on the top surface. Inside this loop, the distance between each cell face center and the current FSW weld position is calculated. If this distance is less than or equal to the radius of the welding tool, heat flux shown by equation (15), is applied to that cell face. Similarly, distance between each cell face center and current laser weld position is calculated. If this distance is less than or equal to laser beam radius, heat flux shown by equation (26) is applied, else convection as well as radiation is applied. Then, UDF is hooked to the FLUENT solver in the same way as explained in chapter 4.

For comparison between the conventional friction stir welding and laser assisted friction stir welding, the maximum temperature in the work piece at location (X=305, Y=5, Z=4) mm is fixed at 400 °C as seen in figure 8.1. Thus in order to maintain the maximum temperature to 400 °C, the heat input to the stir tool was reduced from 1740W to 1000W. It is noted that the maximum temperature in the entire domain does not increase higher than the melting temperature of the work piece material. In the above figure, it can be seen that temperature after 105 seconds for Laser Assisted Friction Stir Welding process is 300 °C which is more than twice the temperature reached during the Friction Stir Welding process. Thus the stirring is taking place in a warmer region, due to the addition of laser pre-heating source, as compared to conventional Friction Stir Welding. Figure 8.2 shows the temperature contours on the top surface of the work piece at time = 60 seconds. In the figure, it can be seen that temperature ahead of the friction stir welding tool is 456 K (i.e. 182.85 °C). By adding preheating source, the temperature ahead of the friction stir tool increases to 618 K (i.e. 344.85 °C), as shown in figure 8.3. Potentially, energy demand by the stir tool is reduced with consequent reduction in tool wear.

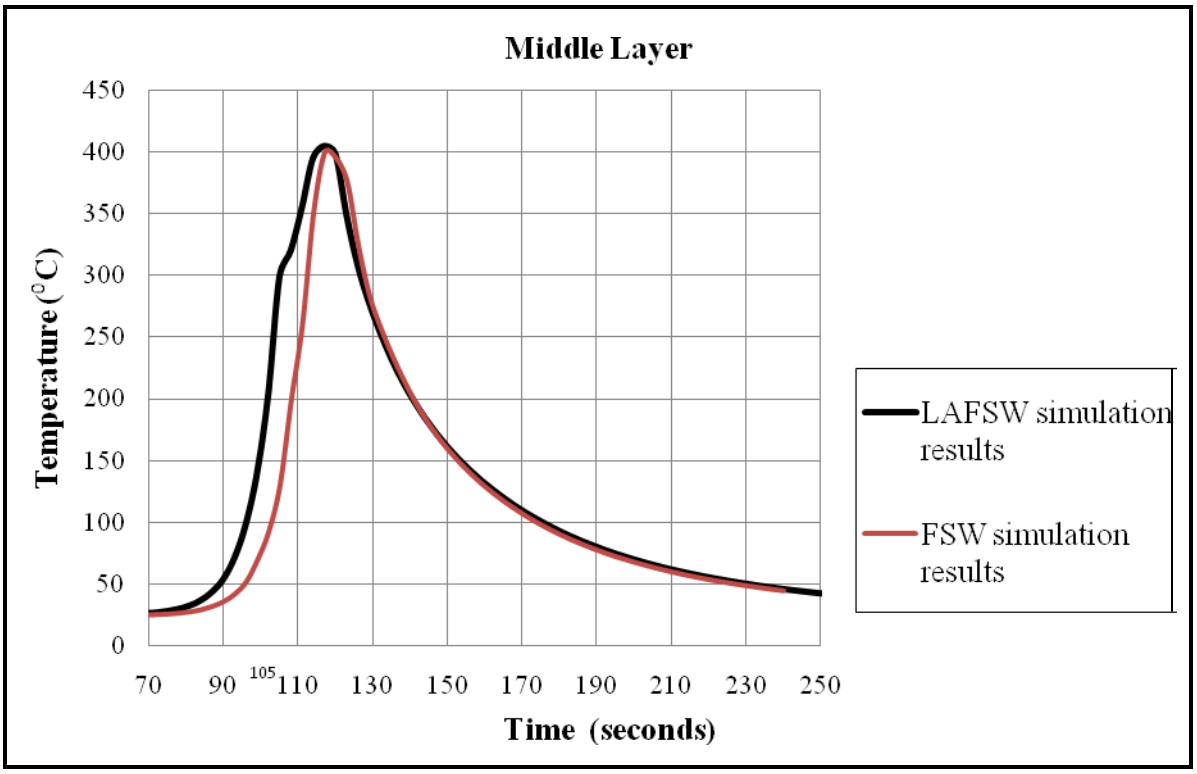

Figure 8.1 Comparison of simulation results of laser assisted friction stir welding and conventional friction stir welding at point (X=305, Y=5, Z=4)

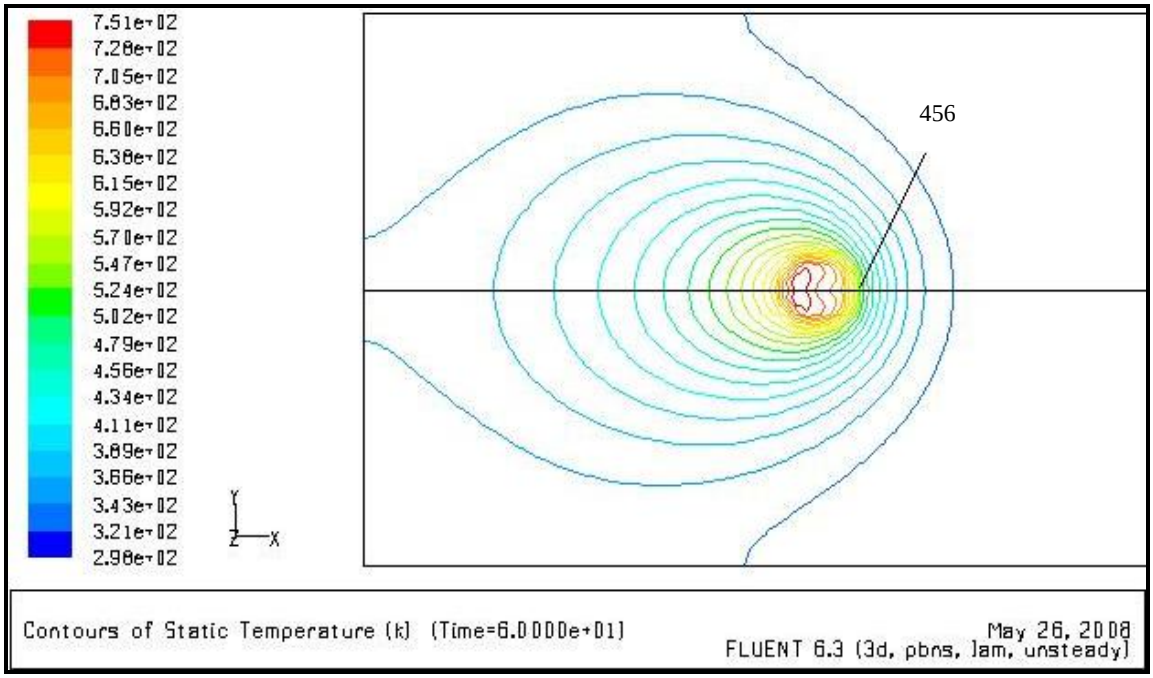

Figure 8.2 Temperature contours on top surface for friction stir welding at time = 60 seconds

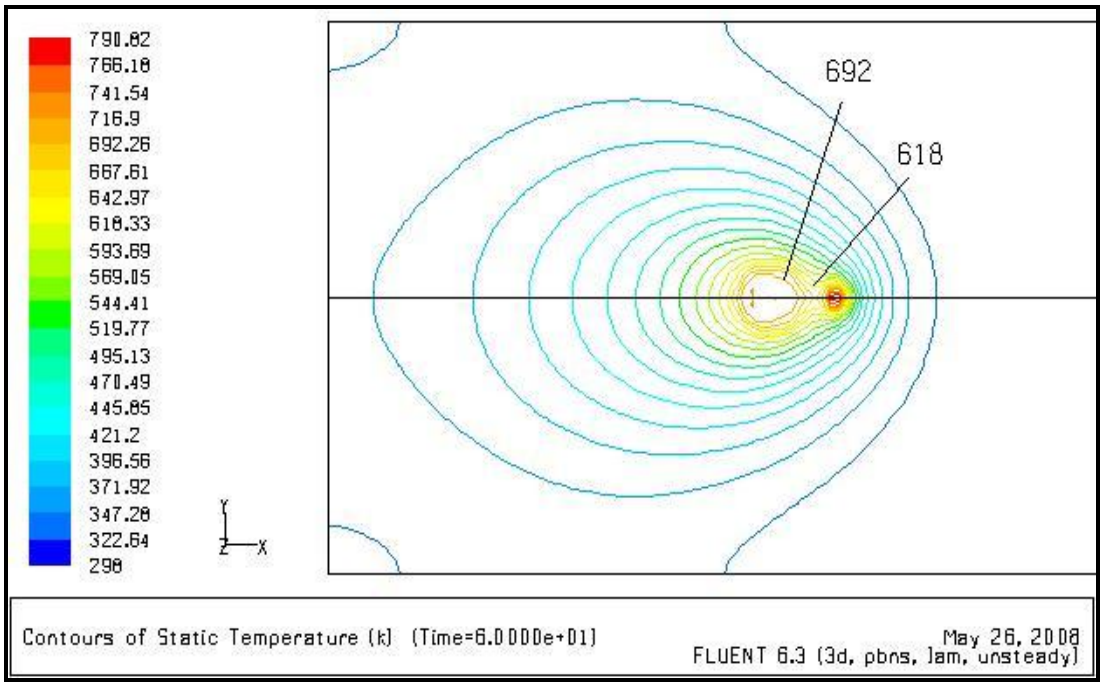

Figure 8.3 Temperature contours on the top surface for laser assisted friction stir welding at time = 60 seconds

Thus if preheating source is added ahead of the friction stir welding tool, less work is required by the stir tool to raise the temperature of the work piece resulting in less downward force on the stir tool.

8.1 Effect of Changing Lead Distances in LAFSW Model

The distance between the center of friction stir welding tool and the point at which pre-heating laser source starts is varied in this section to test its influence on work piece temperature distribution.

For the purpose of current evaluation, LAFSW model for the work piece material of Aluminum alloy-2195 and 304L stainless steel are used. The heat inputs to the top surface of the work piece and the weld feed rate are fixed and lead distance between the two heat sources is varied as given in table 8.1 below. Distances assumed here are arbitrary and they could be varied depending upon the work piece material.

Table 8.1 Model descriptions for varying the lead distance between heat sources

Material	Lead Distance (mm)	FSW heat input (W)	Laser heat input (W)	Feed Rate (mm/s)
Aluminum Alloy 2195	40	1100	600	2.33
	30			
	20			
304L Stainless Steel	40	900	600	1.69
	30			
	20			

Figure 8.4 shows the temperature profiles for different lead distances between the heat sources at location (X=205, Y=5 and Z=4) for aluminum alloy work piece and figure 8.5, shows the temperature profiles for different lead distances between the heat sources at location (X=152, Y=12.7 and Z=0) for 304L stainless steel work piece.

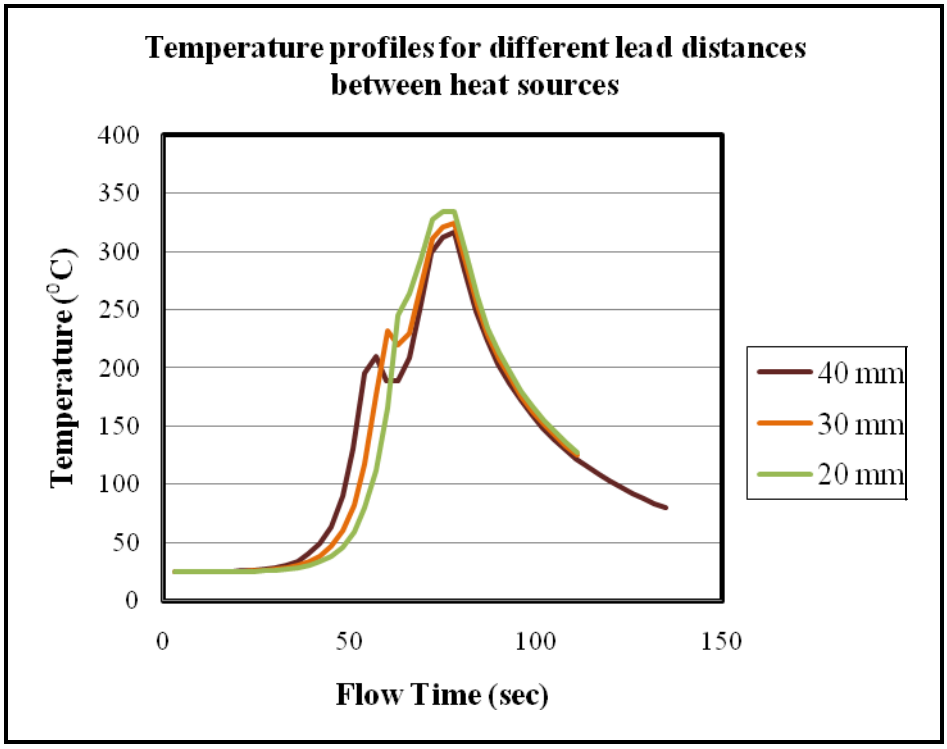

Figure 8.4 Effects of variation of lead distances for aluminum alloy work piece

It can be seen from figures 8.4 and 8.5 that peak temperature in the work piece is highest when the lead distance between the heat sources is the least.

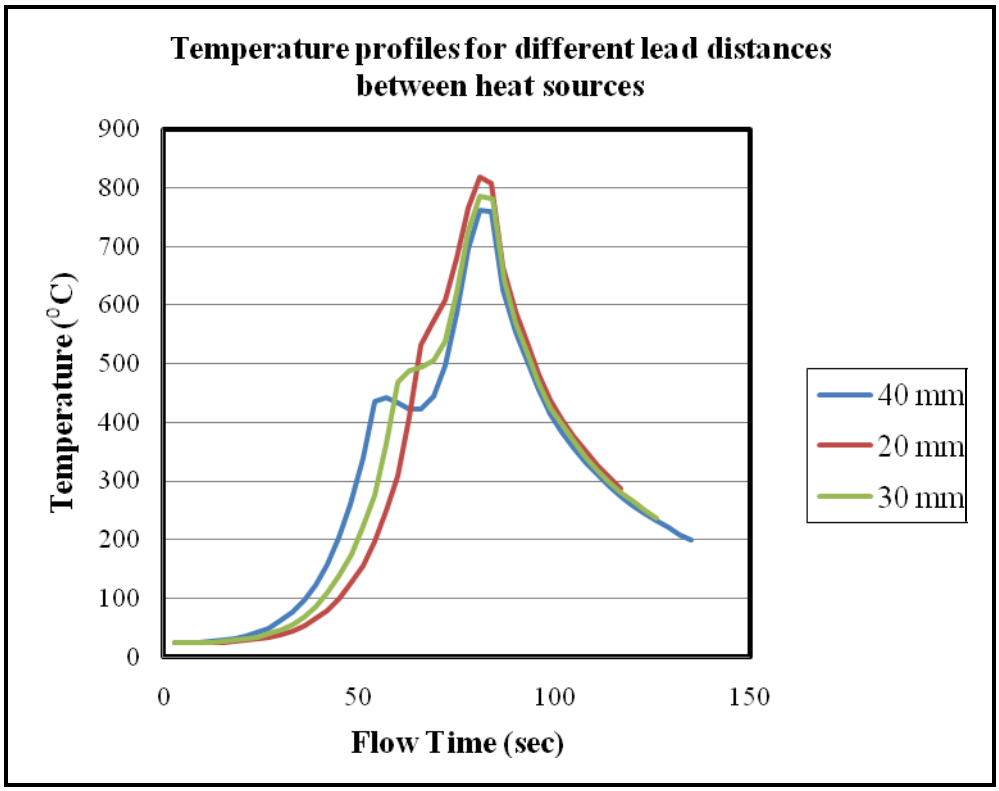

Figure 8.5 Effects of variation of lead distances for 304L stainless steel work piece

It indicates that peak temperature in the work piece increases as lead distance between the heat sources is decreased. Thus in the next sections, shortest feasible distance between the center of friction stir welding tool and the point at which pre-heating laser source starts is applied.

9. Parametric Study of LAFSW Process

9.1 Design of Experiments for LAFSW Process

The results obtained from the developed simulation in chapter 4, correlated well with the experimental results at the top, bottom and middle locations of the work piece. Using the modified friction stir welding model described in chapter 8, which incorporates laser heat source, a parametric study is designed to analyze the controllable parameters with respect to weld quality and LAFSW process productivity. The materials used for the analysis are Al-2195 alloy and 304L stainless steel. The first step in this process is to identify the factors that would be varied. The parameters or control variables considered in this study are tool translational speed, friction stir welding tool heat input and laser heat input. The next step is to determine the levels of these factors. Parameter levels were chosen from within a known operational window obtained from various research papers [22]. The parameter levels were selected so that the effect would be as apparent as possible. Table 9.1 shows the materials and the parameter levels used in this study.

Table 9.1 Laser assisted friction stir welding process parameters used for parametric study

Materials	Feed Rate (mm/sec)	FSW heat input (Watt)	Laser heat input (Watt)
Aluminum alloy-2195	1.5	800	600
	2.33	1000	800
	4.2	1200	1000
304L stainless steel	0.55	400	400
	1.69	500	500
	2.55	900	600

The final step in the parametric process is to perform the experiments and analyze the information. This thesis utilizes a 27-run screening DOE to analyze the effects of 3 input parameters on one selected output. The design consist of 3 independent variables namely feed rate (v), friction stir welding tool heat input (Q_{FSW}) and laser heat input (Q_{laser}), as shown in table 7.1 (a), and 1 dependent (response) variable, work piece temperature (T). The material properties

and boundary conditions applied in the model for parametric design are the same as that applied by Chao, Y.J. and Zhu, X.K. [21] for stainless steel and Chao, Y.J., Qi, X. and Tang, W [8] for Al-2195. The simulation is run 27 times in FLUENT as explained in chapter 4 and peak temperatures were recorded at a point in the work piece which is located at X = 304 mm , Y = 5 mm , Z = 4 mm. Table B.3 in Appendix B, depicts the factors and factor levels and the measured response in screening design.

Similarly, the simulation is run 27 times in FLUENT for stainless steel as explained in chapter 4 and peak temperatures were recorded at a point in the work piece which is located at X = 152 mm, Y = 12.7 mm, Z = 0 mm. Table B.4 in appendix B, depicts the factors and factor levels and the measured response in screening design for stainless steel.

All extracted data was analyzed in Excel and Minitab for multiple linear regression and in Datafit 9.0 for multiple nonlinear regression respectively. It is important to note that any information about the analysis only applies for the range of parameters tested and for this simulation set up. This information may, or may not apply to other LAFSW conditions. Once the input-output data is obtained, to estimate temperature distribution for LAFSW process, regression models were formulated through multiple linear and non linear regression analyses.

9.2 Development of Models for Estimating the Temperature Distribution

9.2.1 Regression Analysis for LAFSW Model of Aluminum Alloy-2195

The simulation data given in B.3 is analyzed in Minitab, statistical software capable of DOE analyses as well as regression analyses. Temperature in the work piece was selected as the dependent variable and three independent variables were used to determine the regression equation. Before performing linear regression in Minitab, the correlation between dependent variables and independent variables was observed. The results of the correlation analysis are

shown in table C.3 in Appendix C. Table C.3 depicts negative correlation coefficient between feed rate and temperature indicating that as feed rate increases, work piece temperature tend to decrease. Figure 9.1 shows numerical simulation results supporting the results obtained from the correlation analysis.

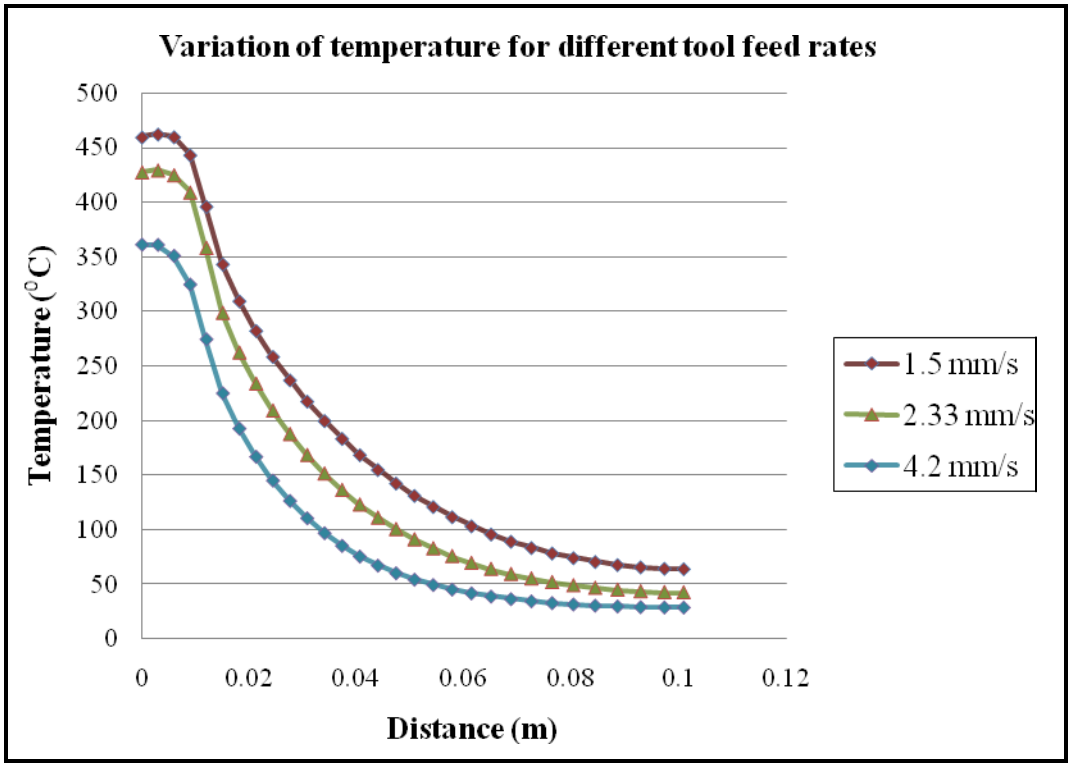

Figure 9.1 Variation of temperature on top surface of Al-2195 for different tool feed rates

Figure 9.1 shows the variation of temperature on top surface of the Al-2195 work piece for linear tool velocities of 1.5 mm/s, 2.33 mm/s and 4.2 mm/s. The temperatures recorded in this figure are taken along a line on the top surface of the work piece at location X = 304 mm and Z = 0. It can be seen from the above graph that highest temperature obtained varies from 470 °C to 360 °C for tool feed rates varying from 1.5 mm /s to 4.2 mm /s respectively, at constant FSW and laser heat input. It can be observed that peak temperature in the work piece reduces as feed rate is increased for a constant value of FSW and laser heat input. From table C.3 in appendix C, it is observed that none of the parameters have a strong linear relationship with the response. Thus it

cannot be asserted that a linear relationship exists between the independent parameters of the LAFSW process and work piece temperature. Since the correlation coefficient depends only on linear relationship between the response and the variable, a more advanced regressor selection procedure is required.

To develop more reliable models, the variables were applied to a regression model and linear regression equation (27) was obtained from the analysis.

$$T = 145 - 31.6 * v + 0.184 * Q_{FSW} + 0.123 * Q_{laser} \quad (27)$$

The complete regression analysis is included in Appendix D. The standardized regression coefficients are listed in table 9.2

Table 9.2 Standardized regression coefficients for Al-2195 work piece temperature

Predictor	**Coefficient**	**SE Coefficient**	**T**	**P**
Constant	-0.000	0.04249	-0.0	1.000
Feed Rate	-0.73952	0.04410	-16.77	0.000
Q_{FSW}	0.43000	0.04400	9.77	0.000
Q_{laser}	0.49733	0.04420	11.25	0.000

These coefficients can be used to interpret the significance of individual independent parameters. As it can be seen from this table, the linear effects of feed rate have the most significant influence on work piece temperature. The simulation data given in B.3 was also analyzed in DataFit version 9.0. A non linear regression equation was obtained as follows,

$$Y = \exp(-0.0954 * v + 0.000533 * Q_{FSW} + 0.000357 * Q_{laser} + 5.260) \quad (28)$$

The complete non linear regression analysis is included in Appendix E.

9.2.2 Regression Analysis for LAFSW Model of 304L Stainless Steel

The simulation data listed in table B.4 is analyzed in Minitab, and the correlation between dependent variables and independent variables was observed. The results of the correlation

analysis are shown in table C.4 in Appendix C. Table C.4 depicts negative correlation coefficient between feed rate and temperature, indicating that as feed rate increases, work piece temperature tends to decrease. Figure 9.2 shows numerical simulation results supporting the results obtained from the correlation analysis.

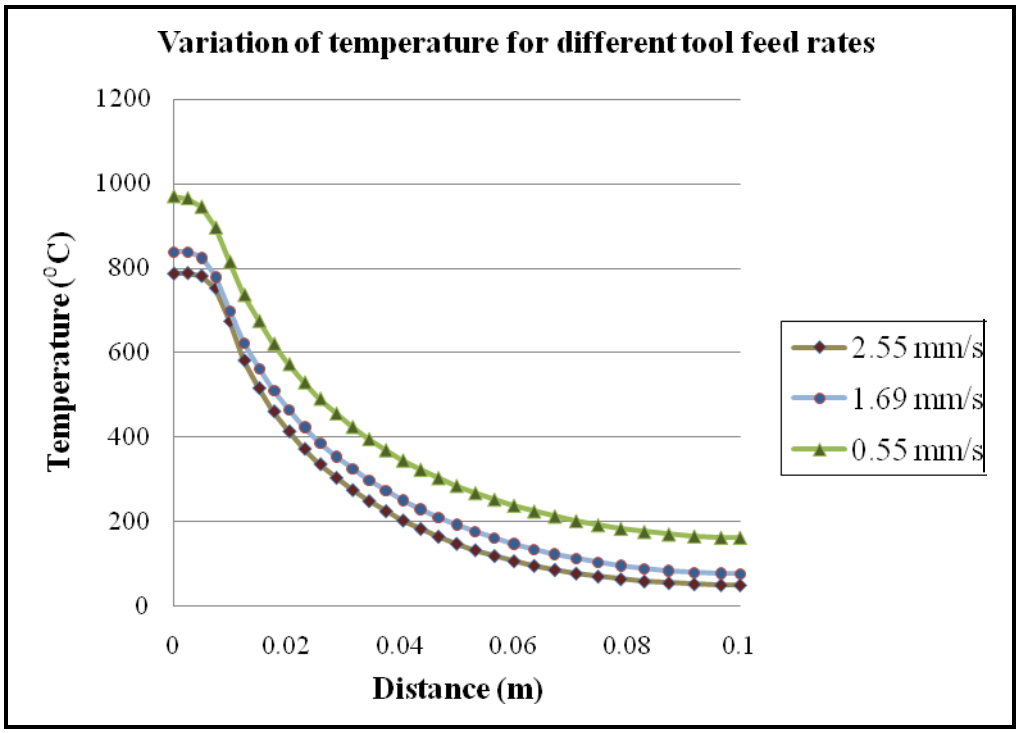

Figure 9.2 Variation of temperature on top surface of 304L stainless steel work piece for different tool feed rates

Figure 9.2 shows the variation of temperature on top surface of the 304L stainless steel work piece for linear tool velocities of 0.55 mm/s, 1.69 mm/s, and 2.55 mm/s. The temperatures recorded in this figure are taken along the centerline on the top surface of the work piece, i.e. at location X = 152 mm and Z = 0. It can be seen from the above graph that highest temperature obtained varies from 790 °C to 990 °C for tool feed rates varying from 0.55 mm /s to 2.55 mm /s respectively, at constant FSW and laser heat input. Thus, peak temperature in the work piece reduces as feed rate is increased for constant values of FSW and laser heat inputs. From table C.4, FSW heat input having a correlation of 0.861, indicates linear relationship with the

response, i.e. work piece temperature. Feed Rate and laser heat input have lower correlation with the work piece temperature. Since it cannot be asserted that a linear relationship exists between the response and the variable, a more reliable model is required. Thus, to develop more reliable models, the variables were applied to a regression model and linear regression equation (29) was obtained from the analysis.

$$T = 163 + (0.435 * Q_{FSW}) + (0.275 * Q_{laser}) - (60.5 * v) \quad (29)$$

The complete regression analysis is included in Appendix D. The standardized regression coefficients are listed in table 9.3.

Table 9.3 Standardized regression coefficients for 304L stainless steel work piece temperature

Predictor	**Coefficient**	**SE Coefficient**	**T**	**P**
Constant	0.000	0.02071	0.00	1.000
Q_{FSW}	0.861	0.0211	40.80	0.000
Q_{laser}	0.206	0.0211	9.76	0.000
Feed Rate	-0.454	0.0211	-21.50	0.000

As it can be seen from this table, the linear effects of FSW heat input have the most significant influence on work piece temperature. Alternatively, a regression analysis was formulated through multiple non linear regression analyses. The simulation data listed in B.4 was analyzed in DataFit version 9.0 and non linear regression equation was obtained as follows,

$$Y = \exp(-0.130 * v + 0.00089 * Q_{FSW} + 0.000563 * Q_{laser} + 5.51) \quad (30)$$

The complete non linear regression analysis is included in Appendix E.

9.3 Estimating Performance of Linear and Non Linear Regression Models for LAFSW Process on Temperature Distribution

The results in Appendix D and E show how accurately the linear and nonlinear models estimated the temperature in the work piece with respect to the changes in tool feed rate, FSW heat input and laser heat input. As mentioned in chapter 6.3, statistical terms such as adjusted coefficient of

determination (R^2_{adj}) are used in this thesis, to obtain the optimal regression model. Other statistical measures like, Durbin-Watson statistic and Akaike's Information Criterion (AIC), as explained in section 6.3, are utilized to study the adequacy of the outcome of the regression analysis. Table 9.4 shows the regression statistics of the LAFSW process for Al -2195 alloy and 304L stainless steel.

Table 9.4 Regression statistics of the LAFSW process for Al -2195 and 304L stainless steel

Process	**Regression Model**	R^2_{adj}	**Durbin-Watson statistic**	**Akaike's Information Criterion (AIC)**
LAFSW of Al -2195	Linear	0.98	1.32	159.764
	Non linear	0.989	1.60	145.2754
LAFSW of 304L stainless steel	Linear	0.988	2.24	186.3585
	Non linear	0.995	1.72	160.5842

Durbin-Watson statistic, values of which are between 0 and 4, is used to determine autocorrelation of the residuals from the regression analysis. Autocorrelation of the residuals indicate that the model can still be improved and leads to biased estimates of statistical significance of the parameters. By comparing the Durbin-Watson values obtained by the regression analysis to the Durbin-Watson significance tables, it is concluded that there is no autocorrelation of the residuals from any of the regression analysis. From table 9.4, it is seen that R^2_{adj} for non linear regression models is higher for both the materials, which indicates that the non linear regression models as given by equations 28 and 30 fits the data better than the linear regression models given by equation 27 and 29 for both Al-2195 and 304L stainless steel. Akaike's information criterion, a measure of the goodness of fit of an estimated statistical model is calculated by equation 22, and the model with the lowest AIC is selected as the best fit model. The lowest AIC statistic was observed for non linear regression models of both the materials, which indicate that non linear regression models given by equation 28 and 30 best fit the data given in Appendix B. Thus the best models for estimating the work piece temperature during the

LAFSW process were the non linear regression models for both Al-2195 alloy and 304L stainless steel.

10. Determining Optimal LAFSW Parameters by Ant Colony Optimization

ACO_R+ algorithm formulated in chapter (7) is used for determining optimal LAFSW parameters. For this study, number of ants: *n*, maximum number of function evaluations: *maxnfe*, a parameter that controls intensification versus diversification: *q*, a positive parameter that has an effect similar to that of the pheromone evaporation rate: ξ, and the size of solution archive: *k*, are fixed at 30, 150,000, 0.7, 0.7 and 15, respectively. To determine the optimal process parameters the optimization models are formulated similar to that in chapter 7. Objective set forth in this thesis is to maximize throughput and minimize cost. Our aim is to seek maximum throughput in minimum cost provided that the weld quality is good. Energy input is the dominant cost component in laser assisted friction stir welding process, as the equipment cost and the labor cost are fixed. Since weld quality is the result of thermal history during welding, the weld quality constraint is equated with temperature constraint. The possible values of process parameters are often limited to the range available in the equipment used for carrying out the process.

In this research, the objective function is obtained by combining the two conflicting objectives as mentioned above. The weights applied to each of the two objectives are assumed equal. As explained in chapter 7, to offset the magnitude difference between the two objectives, the objective with lower magnitude is multiplied by a constant α. Specifically, two optimization models to be solved by the ant colony optimization algorithm can be defined as follows:

Minimize $H - \alpha S$

Subject To: $T_{LB} \leq T \leq T_{UB}$

$H_{LB} \leq H \leq H_{UB}$

$S_{LB} \leq S \leq S_{UB}$

$L_{LB} \leq L \leq L_{UB}$

where *T* is the temperature, *H* is the friction stir welding tool heat input, *S* is the feed rate, and *L* is the laser heat input. *LB* and *UB* stands for lower bound and upper bound respectively.

The two models differ primarily on the equation for T: called Model 1 if linear equations (27) and (29) are used and Model 2 if non linear equations (28) and (30) are used instead, for easy reference later.

10.1 Optimization Results for LAFSW of Al-2195 T8 and 304L Stainless Steel

The ant colony optimization algorithm was applied to solve the optimization model formulated in the previous section for LAFSW of Al2195-T8 by setting α=500, T_{LB} = 425, T_{UB} = 450, H_{LB} = 800, H_{UB} = 1200, L_{LB} = 600, L_{UB} = 1000, S_{LB} = 1.5 and S_{UB} = 4.2. Gradient based nonlinear programming procedure was also applied to solve the formulated optimization model. Due to the stochastic nature of the algorithm, a total of 30 runs were made to generate sufficient statistical data. The best, medium, and worst objective values and CPU time taken are recorded, along with the optimal solution. Table 10.1 summarizes the optimization results by non linear programming and ant colony optimization, for both Model 1 and Model 2, for LAFSW process of Al-2195 T8 and 304L stainless steel materials.

Table 10.1 Optimal solutions for LAFSW of Al2195-T8

		By NP		**By ACO**	
		Model 1	**Model 2**	**Model 1**	**Model 2**
Objective Value	Best	190.506	131.0608	190.506	131.0608
	Median	190.506	131.0608	190.506	131.0608
	Worst	190.506	131.0608	190.508	132.668
Best Solution	FSW Heat Input	1200	1200	1200	1200
	Welding Speed	2.019	2.138	2.019	2.138
	Laser heat input	1000	1000	1000	1000
CPU time	Best	0.0468	0.0468	22.3	22.86
	Median	0.0780	0.0858	22.3	24.24
	Worst	2.0592	2.0748	23.4	25.22
Number of runs found the best solution		30	30	30	28

Similarly, nonlinear programming procedure and ant colony optimization algorithm was applied to solve the optimization model for LAFSW of 304L stainless steel by setting α=500, T_{LB} = 650, T_{UB} = 700, H_{LB} = 400, H_{UB} = 900, L_{LB} = 400, L_{UB} = 600, S_{LB} = 0.55 and S_{UB} = 2.55. A total of 30 runs were made to generate sufficient statistical data. The best, medium, and worst objective values and CPU time taken are recorded, along with the optimal solution. Table 10.2 summarizes the optimization results by non linear programming and ant colony optimization, for both Model 1 and Model 2.

Table 10.2 Optimal solutions for LAFSW of 304L stainless steel

		By NP		**By ACO**	
		Model 1	**Model 2**	**Model 1**	**Model 2**
Objective Value	Best	325.619	245.629	325.619	245.629
	Median	325.619	245.629	325.619	245.629
	Worst	325.619	245.629	328.67	251.237
Best Solution	Heat Input	900	900	900	900
	Welding Speed	1.148	1.308	1.148	1.308
	Laser heat input	600	600	600	600
CPU time	Best	0.0312	0.0468	21.84	22.18
	Median	0.0780	0.0780	22.87	22.18
	Worst	2.0904	2.0904	24.91	23.41
Number of runs found the best solution		30	30	28	27

Even for LAFSW process, it is observed that, the optimization models are simple enough to be solved by gradient based nonlinear programming procedure. On the other hand, Ant Colony Optimization can be useful to solve more complicated models such as non convex and non differentiable ones where gradient based methods would be ineffective. Thus in this section, optimal process parameters were determined for LAFSW process for both Aluminum Alloy-2195 T8 and 304L Stainless Steel.

11. Verification of Optimal Solutions by Simulation

For comparison, table 11.1 gives the summary of optimal results obtained by ant colony optimization for FSW as well as LAFSW processes.

Table 11.1 Summary of optimal parameters obtained by ant colony optimization

Process	**Material**	**Model 1-Linear**			**Model 2- Nonlinear**		
		FSW heat input (Q_{FSW})	feed rate (v)	Tool diameter ϕ	FSW heat input (Q_{FSW})	feed rate (v)	Tool diameter Φ
FSW	Al-2198 T8	1860	2.9514	19	1860	2.911	19
	304L Stainless Steel	1500	1.346	19	1500	1.334	19
		Model 1-Linear			**Model 2-Nonlinear**		
		FSW heat input (Q_{FSW})	feed rate (v)	Laser heat input Q_{laser}	FSW heat input (Q_{FSW})	feed rate (v)	Laser heat input Q_{laser}
LAFSW	Al-2198 T8	1200	2.019	1000	1200	2.138	1000
	304L Stainless Steel	900	1.148	600	900	1.308	600

The following figures illustrate simulation results for the optimal process parameters of FSW and LAFSW process, for both the materials: Aluminum Alloy - 2195 T8 and 304L Stainless Steel. Simulation results for the optimal parameters are compared with statistically obtained optimum results for verification. Figures 11.1, 11.2 and 11.3 show the temperature contours for Aluminum Alloy - 2195 T8 alloy during the FSW process, obtained at 3 sec, 60 sec and 200 sec respectively, for the optimal parameters listed in table 11.1. Figure 11.4 shows temperature history plots for Aluminum Alloy - 2195 T8 alloy, during the FSW process, at location X = 304 mm, Y = 5 mm, Z = 4 mm, for optimal process parameters determined previously. As seen in figure 11.4, with optimal process parameters, peak temperature obtained in case of Al-2195 is 439.9°C. Note that the peak temperature value for the optimal solution is 450°C, according to equation (19).

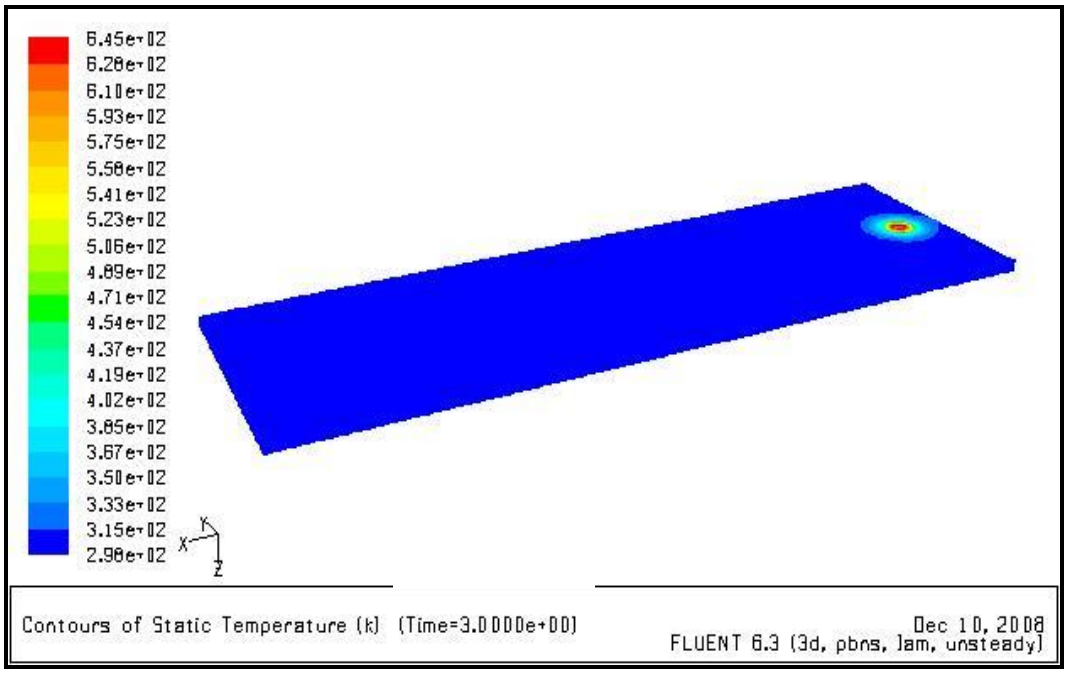

Figure 11.1 Temperature contours for FSW of Al-2195 after 3 sec with optimal parameters as Q_{FSW} =1860 W, v = 2.91 mm/sec and ϕ = 19 mm

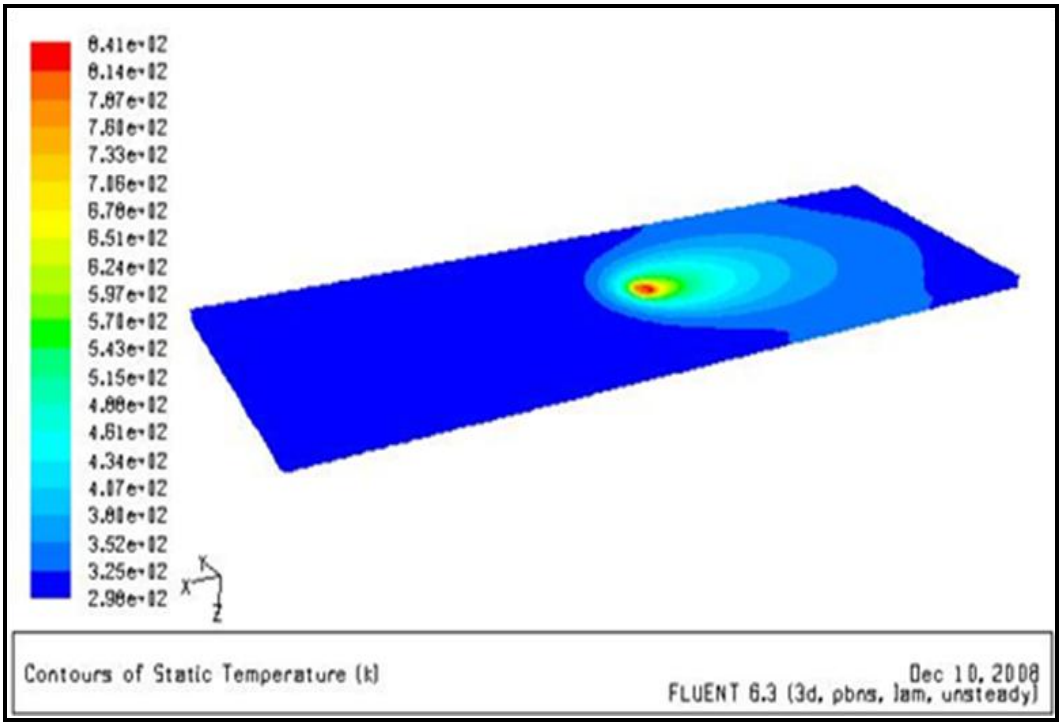

Figure 11.2 Temperature contours for FSW of Al-2195 after 60 sec with optimal parameters as Q_{FSW} =1860 W, v = 2.91 mm/sec and ϕ = 19 mm

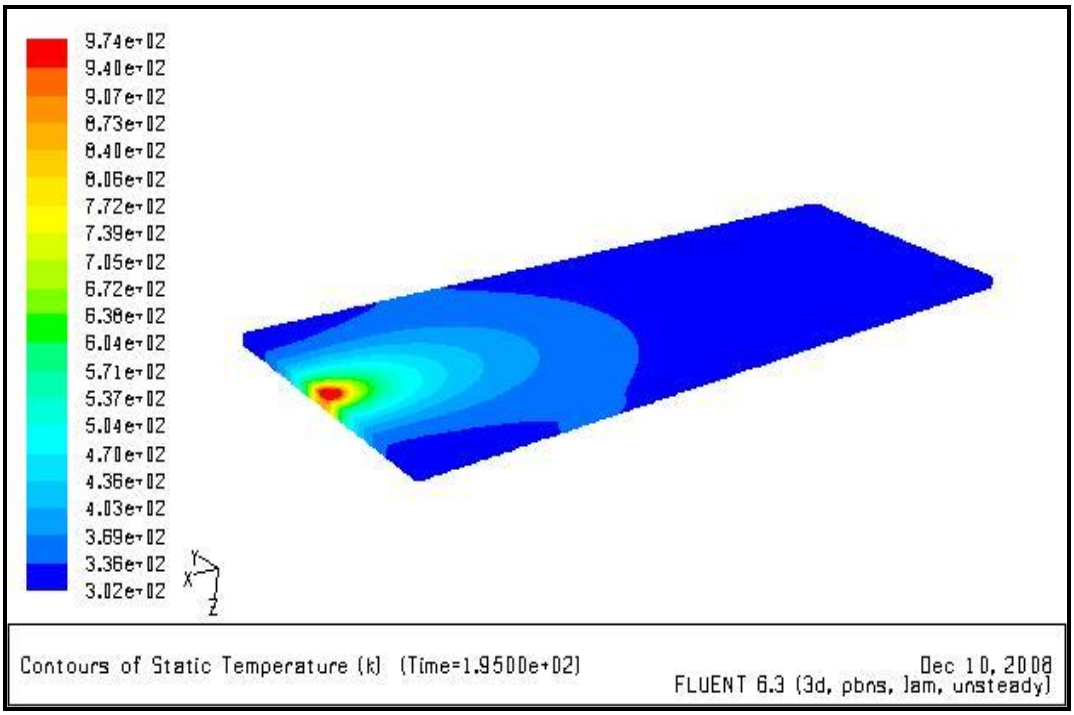

Figure 11.3 Temperature contours for FSW of Al-2195 after 200 sec with optimal parameters as Q_{FSW} =1860 W, v = 2.91 mm/sec and ϕ = 19 mm

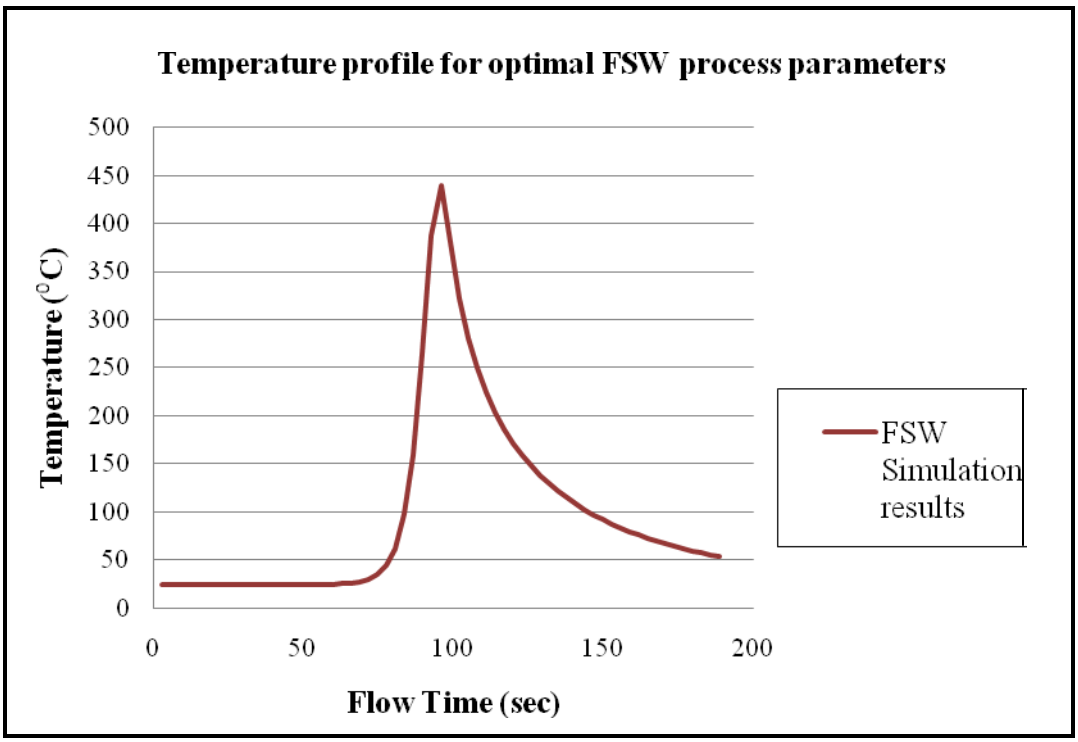

Figure 11.4 Temperature profile at X = 304, Y = 5, Z = 4 for FSW of Al-2195, for optimal parameters as Q_{FSW} =1860 W, v = 2.91 mm/sec and ϕ = 19 mm

Similarly, figure 11.5 shows temperature history plots for 304L stainless steel, during the FSW process, at location X = 152 mm, Y = 12.7 mm, Z = 0 mm, for optimal process parameters determined previously. As seen in figure 11.5, with optimal process parameters, peak temperature obtained in case of 304L stainless steel is 754.5°C. Note that the peak temperature value for the optimal solution is 750 °C, according to equation (21).

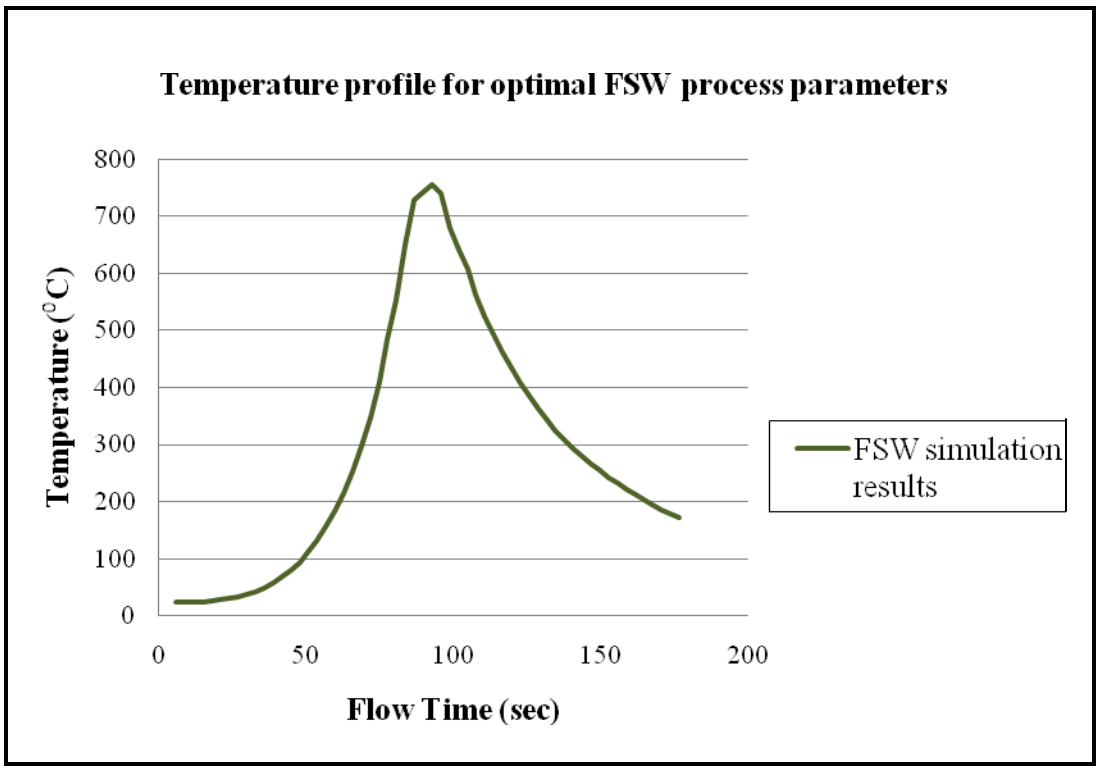

Figure 11.5 Temperature profile at X = 152, Y = 12.7, Z = 0 for FSW of 304L stainless steel, for optimal parameters as Q_{FSW} =1500 W, v = 1.334 mm/sec and ϕ = 19 mm

Figures 11.6, 11.7 and 11.8 show the temperature contours for Al-2195 T8 alloy during the LAFSW process, obtained at 3 sec, 80 sec and 250 sec respectively, for the optimal parameters listed in table 11.1. Figure 11.9 shows temperature history plots for Al-2195 T8 alloy, during the LAFSW process, at location X = 304 mm, Y = 5 mm, Z = 4 mm, for optimal process parameters determined previously. As seen in figure 11.9, with optimal process parameters, peak

temperature obtained in case of Al-2195 is 413.40 °C. Note that the peak temperature value for the optimal solution is 425 °C, according to equation (28).

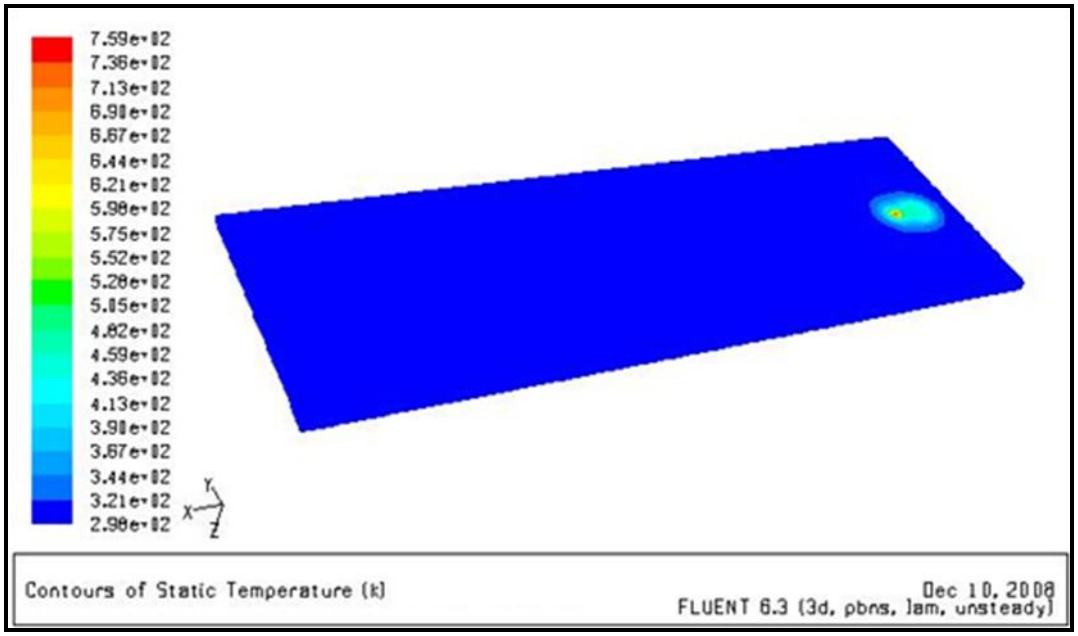

Figure 11.6 Temperature contours for LAFSW of Al-2195 after 3 sec for optimal parameters: Q_{FSW} =1200 W, v = 2.138 mm/sec and Q_{laser} = 1000 W

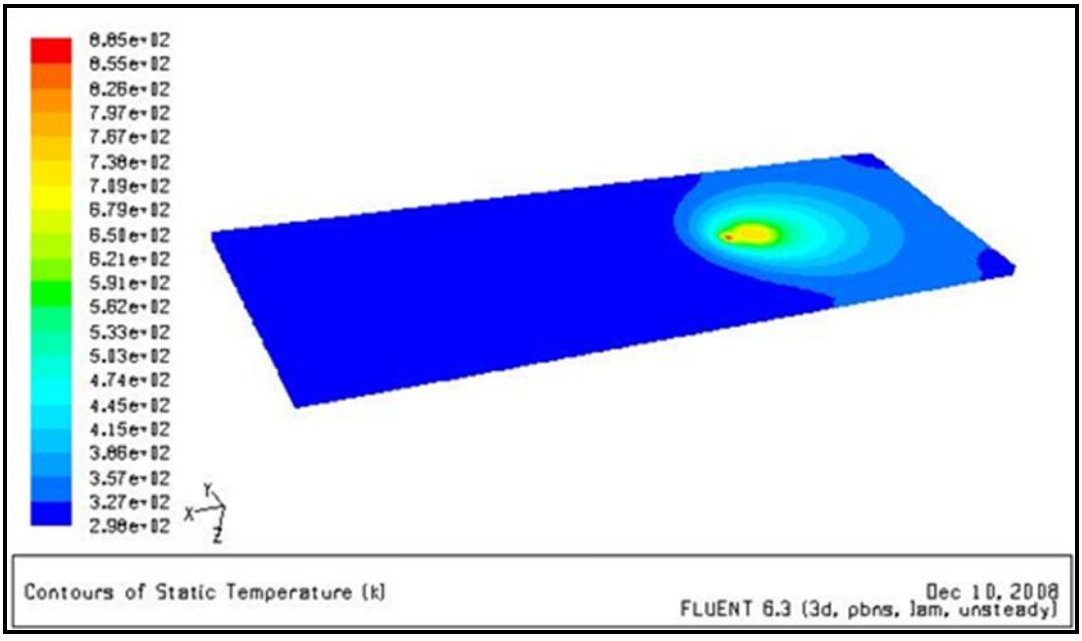

Figure 11.7 Temperature contours for LAFSW of Al-2195 after 80 sec for optimal parameters: Q_{FSW} =1200 W, v = 2.138 mm/sec and Q_{laser} = 1000 W

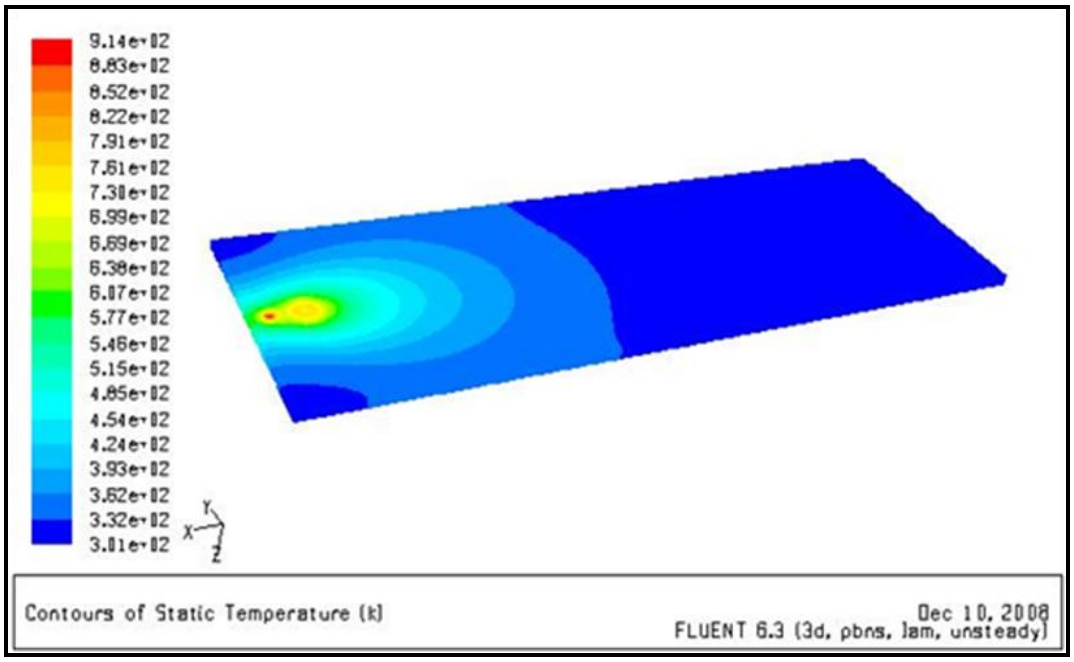

Figure 11.8 Temperature contours for LAFSW of Al-2195 after 250 sec for optimal parameters: Q_{FSW} =1200 W, v = 2.138 mm/sec and Q_{laser} = 1000 W

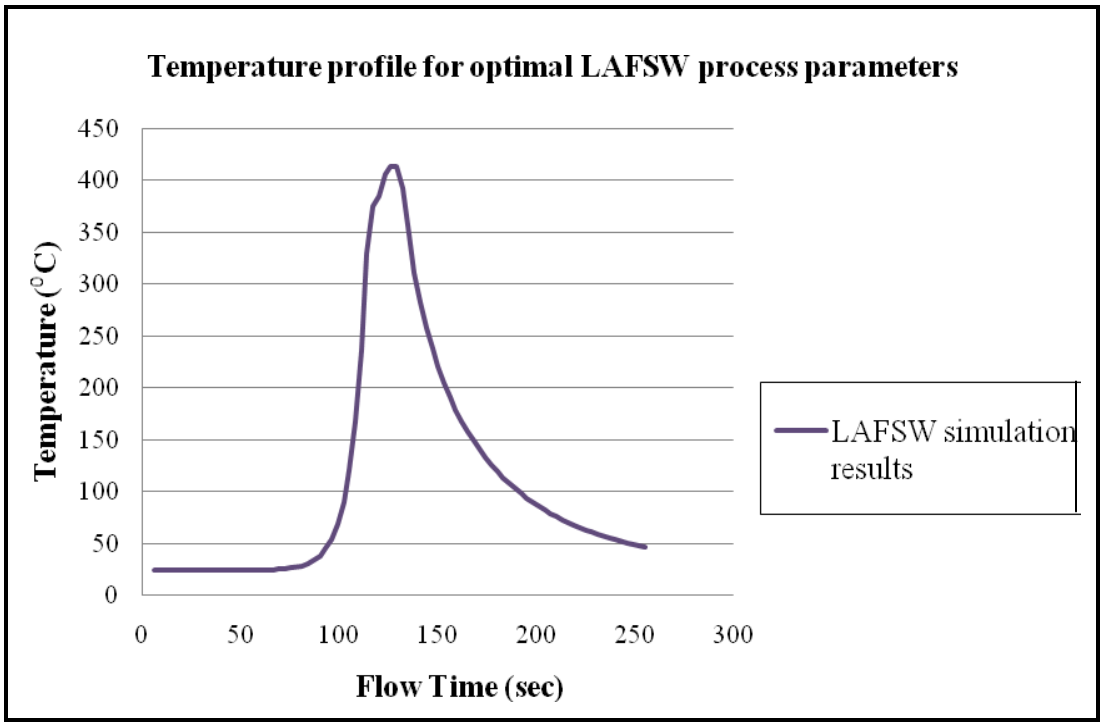

Figure 11.9 Temperature profile at X = 304, Y = 5, Z = 4 for LAFSW of Al-2195, for optimal parameters as Q_{FSW} =1200 W, v = 2.138 mm/sec and Q_{laser} = 1000 W

Similarly, figure 11.10 shows temperature history plots for 304L stainless steel, during the LAFSW process, at location X = 152 mm, Y = 12.7 mm, Z = 0 mm, for optimal process parameters determined previously. As seen in figure 11.10, with optimal process parameters, peak temperature obtained in case of 304L stainless steel is 652.9 °C. Note that the peak temperature value for the optimal solution is 650 °C, according to equation (30).

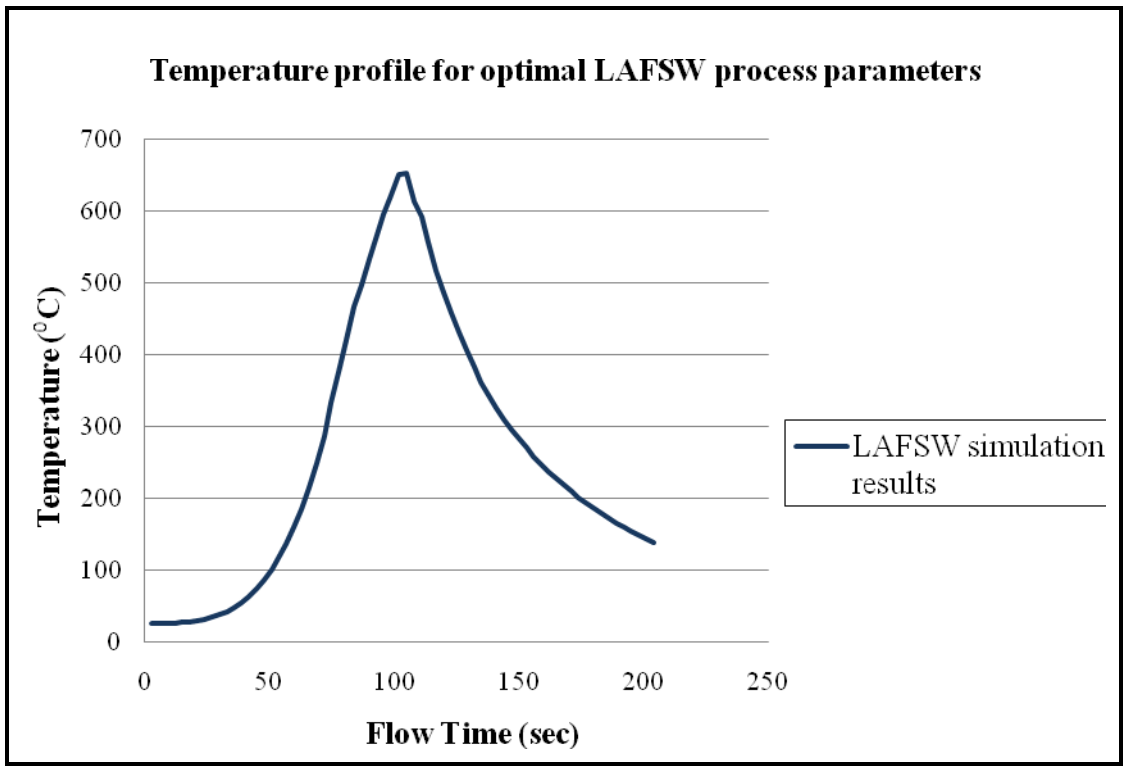

Figure 11.10 Temperature profile at X = 152, Y = 12.7, Z = 0 for 304L stainless steel, for optimal parameters as Q_{FSW} =900 W, v = 1.308 mm/sec and Q_{laser} = 600 W

12. Conclusions and Recommendations for Future Work

The main goal of this study was to develop a transient thermal model for LAFSW process and obtain the optimal parameters for the process. To this end, the existing friction stir welding models of Chao, Qi and Tang [8] and Zhu X.K. and Y.J. Chao [21] were first replicated and then modified to incorporate laser pre-heating. For determining the temperature distribution in the work piece, numerical transient thermal models were developed for FSW of Al -2195 T8 alloy as well as 304L stainless steel using the FLUENT software. Limitations of the FSW model developed were that they were fit to match the unknown thermal contact conductance between the work piece and the backing plate. Further studies could involve experimentally determining the heat transfer coefficient between work piece and backing plate.

Once the models were developed, a screening design of experiments (DOE) was performed to identify the effect of various weld inputs like: feed rate, FSW heat input and FSW tool diameter on temperature distribution in the work piece. The input-output data obtained from the DOE was used in determining the relationship between the process inputs and work piece temperature. Then, regression analysis was performed, and the best fit model was selected for each material. Finally, the optimal combination of friction stir welding parameters is determined by the Ant Colony Optimization method. Based on the models developed, the parametric studies and the optimization results, the following conclusions can be drawn:

1. The effect of FSW tool feed rate has been studied for materials like Al-2195 T8 and 304L stainless steel. Higher work piece temperature is obtained as tool feed rate is reduced.
2. It was also observed that feed rate and FSW heat input have more significant influence on the work piece temperature than FSW tool diameter.

3. FSW process parameters such as feed rate, heat input and tool diameter, have a non linear relationship with work piece temperature, as the non linear regression model best fits the data obtained by simulation results.
4. The optimum parameters for the FSW process were obtained and summarized in table 10.3.

Once the FSW models were developed, laser pre-heating source was added to the existing FSW model. Potential benefits of LAFSW process were also discussed by comparing the LAFSW process with traditional FSW process. A screening design of experiments (DOE) was performed to identify the effect of various process inputs like: feed rate, FSW heat input and laser heat input on temperature distribution in the work piece. The input-output data obtained from the DOE was used in determining the relationship between the process inputs and work piece temperature. The best fit model was selected for each material by regression analysis. Finally, the optimal combination of laser assisted friction stir welding parameters was determined by the Ant Colony Optimization method. Based on the models developed, the parametric studies and the optimization results, the following conclusions can be drawn:

1. It was observed that, if preheating source is added ahead of the friction stir welding tool, less work is required by the stir tool to raise the temperature of the work piece resulting in less downward force on the stir tool. Thus, energy demand by the stir tool is reduced which is expected to result in consequent reduction in tool wear as well.
2. The effect of varying the distance between the center of friction stir welding tool and the point at which pre-heating laser source starts, is studied to test its influence on work piece temperature distribution. The peak temperature in the work piece is the highest when the lead distance between the heat sources is the least.

3. The relationship between the input and output parameters of the LAFSW process is non linear.
4. It is observed that FSW tool feed rate has the highest influence on the work piece temperature, followed by FSW heat input and laser heat input.
5. The optimum parameters for the LAFSW process were obtained and summarized in table 11.1. These optimal solutions were successfully verified by the simulated results obtained by running the transient thermal models.

For future work, experimental observations need to be performed to verify the numerical simulations developed in this thesis. The thermal model used in this research assumes that friction between tool shoulder and work piece is the only heat generation source. More comprehensive heat generation models could be developed to include the effects of plastic deformation of the work piece as well. Similar experiments could be performed for the consideration of several other process parameters like plunge depth, dwell time etc. The effect of process parameters on mechanical properties of the work piece could also be determined next, if an uncoupled or coupled mechanical model is incorporated.

Bibliography

1. Record, J.H., *Statistical Investigation of Friction Stir Processing Parameter Relationships*, in *Mechanical Engineering*. 2005, Brigham Young University, p. 1-63.

2. Chao, Y.J. and X.H. Qi, *Thermal and thermo-mechanical modeling of friction stir welding of aluminum alloy 6061-T6* Journal of Materials Processing & Manufacturing Science, 1999. 7(2): p. 215-233.

3. Lienert, T.J., Stellwag, W.L., Grimmett, B.B. and Warke, R.W., *Friction stir welding studies on mild steel - Process results, microstructures, and mechanical properties are reported* Welding Journal, 2003, **82**(1): p. 1S-9S.

4. Kohn, G., Greenberg, Y., Makover, I. and Munitz, A., *Laser-assisted friction stir welding*, Welding Journal, 2002. **81**(2): p. 46-48.

5. Reynolds, A.P., Tang, W., Khandkar, Z., Khan, J.A. and Lindner, K., *Relationships between weld parameters, hardness distribution and temperature history in alloy 7050 friction stir welds* Science and Technology of Welding and Joining, 2005. **10**(2): p. 190-199.

6. Naidu, R., *Friction Stir Welding: Thermal Effects of a parametric study on Butt and Lap welds*, in *Mechanical Engineering* 2006, Wichita State University. p. 1-78.

7. Gould, J.E. and Z.L. Feng, *Heat flow model for friction stir welding of aluminum alloys* Journal of Materials Processing & Manufacturing Science, 1999. **7**(2): p. 185-194.

8. Chao, Y.J., X. Qi, and W. Tang, *Heat transfer in friction stir welding - Experimental and numerical studies*, Journal of Manufacturing Science and Engineering-Transactions of the ASME, 2003. **125**(1): p. 138-145.

9. Khandkar, M.Z.H., J.A. Khan, and A.P. Reynolds, *Prediction of temperature distribution and thermal history during friction stir welding: input torque based model*, Science and Technology of Welding and Joining, 2003. **8**(3): p. 165-174.

10. Song, M. and R. Kovacevic, *Thermal modeling of friction stir welding in a moving coordinate system and its validation*, International Journal of Machine Tools & Manufacture, 2003. **43**(6): p. 605-615.

11. Long, X. and S.K. Khanna, *Modeling of electrically enhanced friction stir welding process using finite element method*, Science and Technology of Welding and Joining, 2005. **10**(4): p. 482-487.

12. Rozzi, J.C., Pfefferkorn, F.E., Incropera, F.P. and Shin, Y.C., *Transient, three-dimensional heat transfer model for the laser assisted machining of silicon nitride: I.*

Comparison of predictions with measured surface temperature histories, International Journal of Heat and Mass Transfer, 2000. **43**(8): p. 1409-1424.

13. Jeon, Y. and F. Pfefferkorn, *Effect of laser preheating the work piece on micro end milling of metals,* Journal of Manufacturing Science and Engineering-Transactions of the ASME, 2008. **130**(1)

14. Schuocker, D., *Mathematical modeling of laser-assisted deep drawing,* Journal of Materials Processing Technology, 2001. **115**(1): p. 104-107.

15. M. Merklein, A.G., *Laser assisted Friction Stir Welding of drawable steel-aluminum tailored hybrids.* Int J Mater Form, 2008: p. 1-4.

16. J.H Record, J.L.C., T.W Nelson, C.D Sorensen, and B.W Webb *A Look at the Statistical Identification of Critical Process Parameters in Friction Stir Welding,* Welding Journal, 2007: p. 97-103.

17. Christian, B. and R. Andrea, *Metaheuristics in combinatorial optimization: Overview and conceptual comparison* ACM Comput. Surv., 2003. **35**(3): p. 268-308.

18. Kim, D., S. Rhee, and H. Park, *Modeling and optimization of a GMA welding process by genetic algorithm and response surface methodology,* International Journal of Production Research, 2002. **40**(7): p. 1699 - 1711.

19. Tarng, Y.S., H.L. Tsai, and S.S. Yeh, *Modeling, optimization and classification of weld quality in tungsten inert gas welding,* International Journal of Machine Tools & Manufacture, 1999. 39(9): p. 1427-1438.

20. Sathiya, P., Aravindan, S., Haq, A.N. and Panneerselvam, K., *Optimization of friction welding parameters using simulated annealing,* Indian Journal of Engineering and Materials Sciences, 2006. **13**(1): p. 37-44.

21. Zhu, X.K. and Y.J. Chao, *Numerical simulation of transient temperature and residual stresses in friction stir welding of 304L stainless steel,* Journal of Materials Processing Technology, 2004. **146**(2): p. 263-272.

22. Nandan, R., Roy, G.G., Lienert, T.J. and DebRoy, T., *Numerical modeling of 3D plastic flow and heat transfer during friction stir welding of stainless steel,* Science and Technology of Welding and Joining, 2006. **11**(5): p. 526-537.

23. H. R. Shercliff, M.J.R., Adam Taylor and T.L. Dickerson, *Micro structural Modeling in Friction Stir Welding of 2000 series Aluminum Alloys,* Mecanique and Industries, 2005. **6**: p. 25-35.

24. Dorigo, M., Socha, K., *Ant colony optimization for continuous domains,* European Journal of Operational Research, 2008. **185**: p. 1155-1173.

25. Deb, K., *An efficient constraint handling method for genetic algorithms*, Computer Methods in Applied Mechanics and Engineering, 2000. **186**: p. 311-338.

26. Kohn, G., *Process and Apparatus for Friction Stir Welding*, in *United States Patent Application Publication*. 2005: USA.

27. Chang, W.S. and S.J. Na, *A study on heat source equations for the prediction of weld shape and thermal deformation in laser micro welding* Metallurgical and Materials Transactions B-Process Metallurgy and Materials Processing Science, 2002. **33**(5): p. 757-764.

28. Lakshminarayanan, A.K. and V. Balasubramanian, *Process parameters optimization for friction stir welding of RDE-40 aluminum alloy using Taguchi technique* Transactions of Nonferrous Metals Society of China, 2008. 18(3): p. 548-554.

Appendix A: User Defined Function

A.1 UDF for Specifying Moving Heat Flux for Friction Stir Welding

```
#include "udf.h"
DEFINE_PROFILE (Heat_Flux,t,i)
{
real x[ND_ND], A[ND_ND], c[ND_ND], rcal[ND_ND], Atotal[ND_ND];  /* this will hold the
position vector */
face_t f;
real current_time, dt;
real vel;
real r,q,qt,y;
int abst;
current_time = RP_Get_Real("flow-time");  // sec
dt = RP_Get_Real("physical-time-step");
vel = 2.33e-3;  // m per sec
c[0] =0.020+ 0.0127  + vel * current_time ;
c[1] = 0;
c[2] = 0;  // c = center of the weld position vector
Atotal[0] = 0;Atotal[1] = 0;Atotal[2] = 0;
qt = 0;
begin_f_loop(f,t)
   {
     F_CENTROID(x,f,t);
```

```
    NV_VV(rcal, =, x, -, c);
    r = NV_MAG(rcal);
    if (r < 0.0127 &&  r> 0)
        {
                q = (3*1740*r)/(2*3.14*(pow(0.0127,3)));  //w/m2
                F_PROFILE(f,t,i) = q;
                F_AREA(A,f,t);
                qt = qt + q* NV_MAG(A);
                printf("q Areas = %f %f  %f  %f  \n", q, A[0],A[1],A[2]);
                NV_VV(Atotal, = ,Atotal, +, A);
        }
      else
        {
                 F_PROFILE (f,t,i) = -30*(F_T(f,t) -298);  //w/m2
                 y = F_T (f,t);
         }
   }
end_f_loop(f,t)
printf("\n Qt diff = %f \n", qt );
}
```

A.2 UDF for Specifying Moving Heat Flux for Laser Assisted Friction Stir Welding

```
#include "udf.h"
DEFINE_PROFILE (Heat_Flux,t,i)
```

```
{
real x[ND_ND], A[ND_ND], c[ND_ND], h[ND_ND], lrcal[ND_ND], rcal[ND_ND],
Atotal[ND_ND];   /* this will hold the position vector */
face_t f;
real current_time, dt;
real vel;
real r,lr,d,p,q,qt,y,m;
int abst;
current_time = RP_Get_Real("flow-time");  // sec
dt = RP_Get_Real("physical-time-step");
vel = 2.33e-3;
c[0] = 0.020 +0.0127  + vel * current_time ; // 20mm left as starting length and 0.0127 is the
radius of the weld
c[1] = 0;
c[2] = 0;  // c = center of the weld position vector
h[0] = 0.02 + 0.0127 + 0.020 + 0.005 +vel * current_time ; // laser heat source center
h[1] = 0;
h[2] = 0;
Atotal [0] = 0; Atotal [1] = 0; Atotal [2] = 0;
qt = 0;
begin_f_loop(f,t)
   {
        F_CENTROID(x,f,t);
```

```
NV_VV(rcal, =, x, -, c);
NV_VV(lrcal, =, x, -, h);
r = NV_MAG(rcal);
lr = NV_MAG(lrcal);
if (r < 0.0127 &&  r> 0)
    {
        q = (3*1300*r)/(2*3.14*(pow(0.0127,3)));  //w/m2-FSW heat flux
        F_PROFILE(f,t,i) = q;
     }
else if (lr < 0.005 && lr > 0)
    {
        d = ((2*800)/(3.14*(pow(0.005,2))));
        p = ((-2*(pow(lr,2)))/(pow(0.005,2)));
        q = d*(exp (p)); // w/m2 laser heat flux
        F_PROFILE (f,t,i) = q;
        F_AREA(A,f,t);
        qt = qt + q* NV_MAG(A);
        printf("q Areas = %f %f  %f  %f  \n", m,q, A[0],A[1],A[2]);
        NV_VV(Atotal, = ,Atotal, +, A);
        }
else
 {
        F_PROFILE(f,t,i) = -30*(F_T(f,t) -298);  //w/m2-convection on top surface
```

```
            y = F_T(f,t);
            F_PROFILE(f,t,i)=-10*(F_T(f,t)-298)-0.000000009639*((pow(y,4))-
            (pow(298,4))); //Radiation and convection together
        }
    }
end_f_loop(f,t)
printf("\n Qt = %e %f \n", qt, m );
}
```

Appendix B: Numerically Produced Data Used for Statistical Analyses

Table B.1 Factors and factor levels of FSW process for Al-2195 alloy with measured response for parametric study

Heat Input (W) Q	**Feed Rate (mm/s)** v	**Tool shoulder diameter(mm)** ϕ	**Temperature (°C)** T
1760	2.33	25.4	408.615
1760	1.5	25.4	451.62
1760	4.2	25.4	348.385
1860	4.2	19	386.71
1500	4.2	19	323.048
1500	1.5	25.4	395.172
1760	2.33	19	447.11
1860	1.5	19	542.6
1500	2.33	19	389.49
1760	1.5	19	516.44
1860	4.2	25.4	347.21
1760	4.2	19	369.002
1860	2.33	19	469.33
1500	2.33	25.4	356.76
1860	1.5	25.4	474.1
1500	4.2	25.4	305.467
1860	2.33	25.4	428.62
1500	1.5	19	448.576

Table B.2 Factors and factor levels of FSW process for 304L stainless steel with measured response for parametric study

Feed Rate (mm/sec) ***v***	**Heat Input (W)** ***Q***	**Tool Diameter (mm)** ϕ	**Temperature (°C)** ***T***
0.55	1000	15	589.55
0.55	1000	19	592.77
0.55	1200	15	693.97
0.55	1200	19	691.15
0.55	1500	15	839.35
0.55	1500	19	837.75
1.69	1000	15	469.71
1.69	1000	19	504.679
1.69	1200	15	549.688
1.69	1200	19	592.04
1.69	1500	15	666.67
1.69	1500	19	720.43
2.55	1000	15	425.06
2.55	1000	19	438.087
2.55	1200	15	497.119
2.55	1200	19	512.12
2.55	1500	15	603.32
2.55	1500	19	624.476

Table B.3 Factors and factor levels of LAFSW process for Al-2195 alloy with measured responses for parametric study

Feed Rate (mm/s) v	**FSW heat input (W)** Q_{FSW}	**Laser heat input (W)** Q_{laser}	**Temp (°C)** T
4.2	1200	600	310.71
4.2	1000	1000	315.53
4.2	1200	1000	347.57
4.2	1000	600	277.77
4.2	800	600	244.38
4.2	800	800	263.81
4.2	1200	800	326.42
4.2	1000	800	295.22
4.2	800	1000	281.65
2.33	1000	600	322.44
2.33	800	800	307.49
2.33	800	600	283.78
2.33	1000	1000	370.05
2.33	1200	600	358.61
2.33	1200	800	384.45
2.33	1200	1000	408.68
2.33	800	1000	342.84
2.33	1000	800	347.07
1.5	800	800	338.9
1.5	1200	1000	451.36
1.5	1200	800	426.52
1.5	1000	600	354.18
1.5	800	1000	377.79
1.5	800	600	310.97
1.5	1000	800	384.52
1.5	1200	600	398.35
1.5	1000	1000	407.71

Table B.4 Factors and factor levels of LAFSW process for 304L stainless steel with measured responses for parametric study

FSW heat input (W) Q_{FSW}	**Laser heat input (W)** Q_{laser}	**Feed Rate (mm/s)** v	**Temp (°C)** T
900	400	0.55	650.1
900	500	0.55	677.58
900	600	0.55	704.53
900	400	1.69	563.45
900	500	1.69	589.01
900	600	1.69	614.29
900	400	2.55	496.91
900	500	2.55	520.71
900	600	2.55	544.33
400	600	2.55	359.03
400	500	2.55	332.41
400	400	2.55	308.27
400	600	1.69	398.15
400	600	0.55	467.65
400	500	1.69	370.27
400	500	0.55	430.24
400	400	1.69	343.93
400	400	0.55	395.01
500	600	2.55	394.31
500	600	1.69	440.53
500	600	0.55	511.02
500	500	2.55	370.25
500	500	1.69	414.43
500	500	0.55	477.21
500	400	2.55	346.1
500	400	1.69	388.15
500	400	0.55	446.06

Appendix C: Correlation Analyses

Table C.1 Correlation analysis matrix for FSW of aluminum alloy

	Heat Input (Q)	**Feed Rate (v)**	**Tool diameter (ϕ)**
Feed Rate (v)	0.00		
	1.00		
Tool diameter (ϕ)	0.00	0.00	
	1.00	1.00	
Temperature (T)	0.477	-0.791	-0.327
	0.045	0.00	0.185

(Note: The values in blue ink indicate p-values)

Table C.2 Correlation analysis matrix for FSW of stainless steel

	Feed Rate (v)	**Heat Input (Q)**	**Tool diameter(ϕ)**
Heat Input (Q)	0.000		
	1.000		
Tool diameter (ϕ)	0.000	0.000	
	1.000	1.000	
Temp (T)	-0.662	0.732	0.084
	0.003	0.001	0.741

(Note: The values in blue ink indicate p-values)

Table C.3 Correlation analysis matrix for LAFSW of aluminum alloy

	Feed Rate (v)	**FSW heat input (Q_{FSW})**	**Laser heat input (Q_{laser})**
FSW heat input (Q_{FSW})	0.00		
	1.00		
Laser heat input (Q_{laser})	0.00	0.00	
	1.00	1.00	
Temperature (T)	-0.697	0.586	0.392
	0.00	0.001	0.043

(Note: The values in blue ink indicate p-values)

Table C.4 Correlation analysis matrix for LAFSW of stainless steel

	FSW heat input (Q_{FSW})	**Laser heat input (Q_{laser})**	**Feed Rate (v)**
Laser heat input (Q_{laser})	0.00		
	1.00		
FSW heat input (Q_{FSW})	0.00	0.00	
	1.00	1.00	
Temperature (T)	0.861	0.206	-0.454
	0.00	0.303	0.017

(Note: The values in blue ink indicate p-values)

Appendix D: Multiple Linear Regression Results

D.1 FSW of Aluminum Alloy- 2195: Minitab Results

The regression equation is:

Temp = 334 + 0.201 Heat Input - 44.7 Feed Rate - 6.53 Tool diameter

Table D.1 Regression variable results

Predictor	Coef	SE Coef	T	P
Constant	333.90	45.65	7.31	0.000
Heat Input	0.20065	0.02234	8.98	0.000
Feed Rate	-44.728	3.002	-14.90	0.000
Tool Diameter	-6.53	1.059	-6.17	0.000

S = 14.3841, R-Sq = 96.1%, R-Sq (adj) = 95.2%, PRESS = 4949.72, R-Sq (pred) = 93.25%

Durbin-Watson statistic = 2.92

Table D.2 Analysis of variance

Source	DF	SS	MS	F	P
Regression	3	70471	23490	113.53	0.000
Residual Error	14	2897	207		
Total	17	73368			

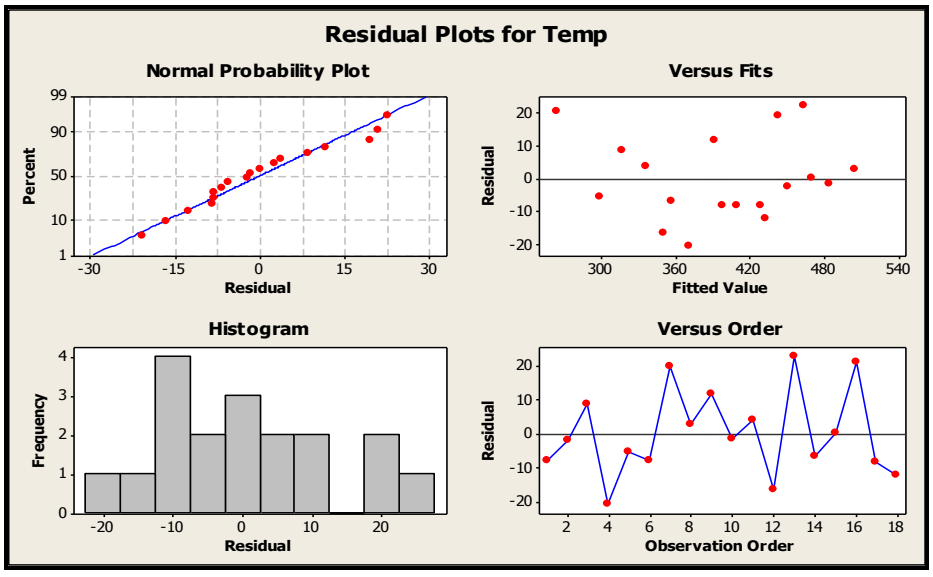

Figure D.1 FSW residuals plot for work piece temperature-Al 2195

D.2 FSW of 304L Stainless Steel: Minitab Results

The regression equation is:

Temp = 149 + 0.424 Heat Input - 96.1 Feed Rate + 4.97 Tool Diameter

Table D.3 Regression variable results

Predictor	Coef	SE Coef	T	P
Constant	148.87	45.74	3.26	0.006
Feed Rate	-96.051	5.251	-18.29	0.000
Heat Input	0.42372	0.0209	20.24	0.000
Tool Diameter	4.974	2.151	2.31	0.036

S = 18.247, R-Sq = 98.2%, R-Sq (adj) = 97.8%, PRESS = 8158.86, R-Sq (pred) = 96.79%

Durbin-Watson statistic = 1.937

Table D.4 Analysis of variance

Source	DF	SS	MS	F	P
Regression	3	249666	83222	249.93	0.000
Residual Error	14	4662	333		
Total	17	254328			

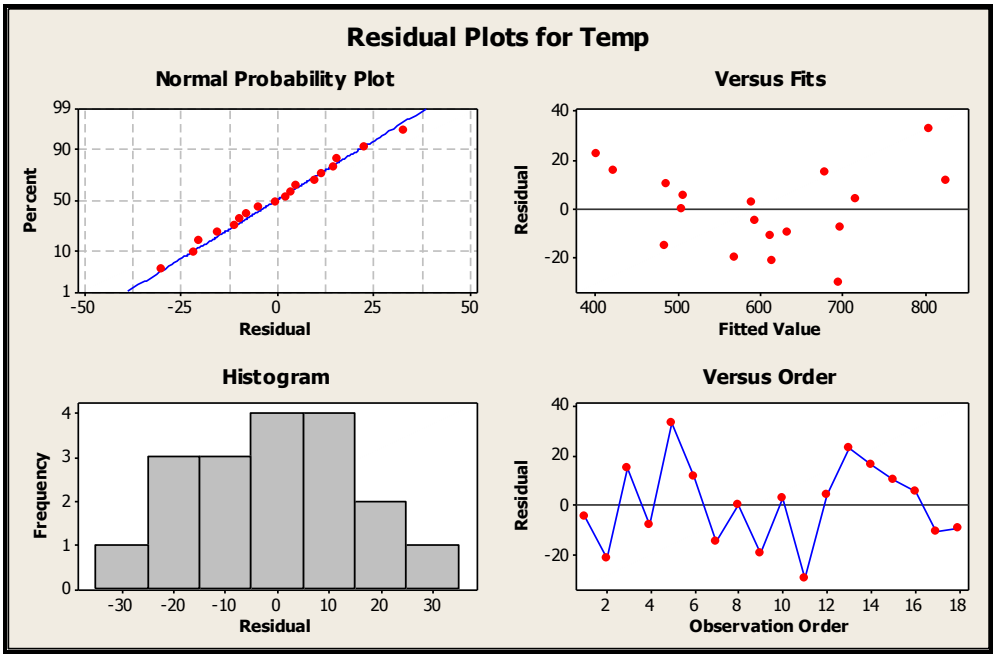

Figure D.2 FSW residuals plot for work piece temperature-304L stainless steel

D.3 LAFSW of Aluminum Alloy-2195: Minitab Results

The regression equation is:

Temp = 145 - 31.6 feed rate + 0.184 FSW + 0.123 laser

Table D.5 Regression variable results

Predictor	Coef	SE Coef	T	P
Constant	144.81	11.63	12.46	0.000
feed rate	-31.562	1.247	-25.30	0.000
FSW	0.183628	0.008626	21.29	0.000
laser	0.122775	0.008626	14.23	0.000

S = 7.31952, R-Sq = 98.3%, R-Sq (adj) = 98.0%, PRESS = 1749.32, R-Sq (pred) = 97.52%

Durbin-Watson statistic = 1.32210

Table D.6 Analysis of variance

Source	DF	SS	MS	F	P
Regression	3	69426	23142	431.95	0.000
Residual Error	23	1232	54		
Total	26	70658			

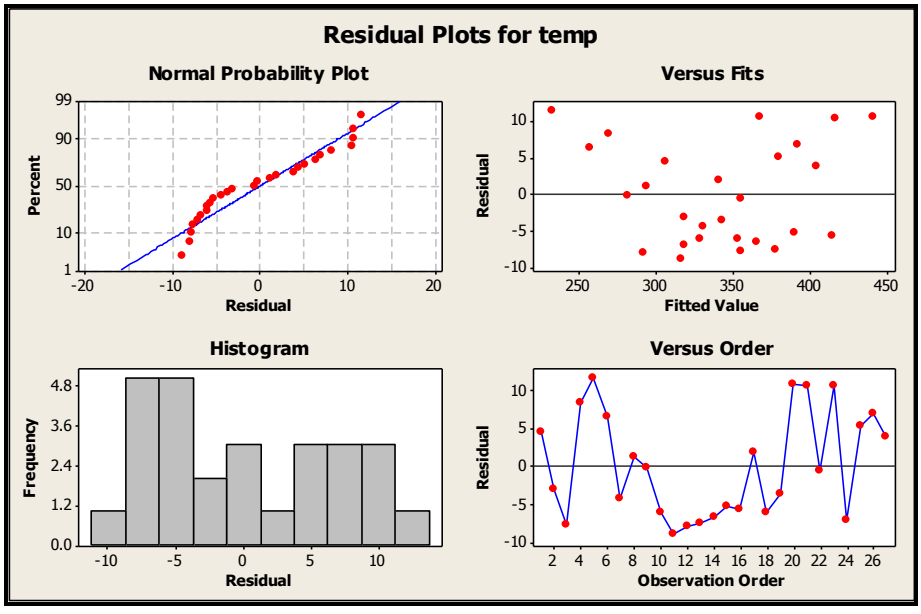

Figure D.3 LAFSW residuals plot for work piece temperature- Al 2195

D.4 LAFSW of 304L Stainless Steel: Minitab Results

The regression equation is:

Temp = 163 + 0.435 FSW heat input + 0.275 Laser heat input - 60.5 Feed rate

Table D.7 Regression variable results

Predictor	Coef	SE Coef	T	P
Constant	162.62	16.30	9.98	0.000
FSW heat input	0.43530	0.01067	40.80	0.000
Laser heat input	0.27548	0.02823	9.76	0.000
Feed rate	-60.484	2.814	-21.50	0.000

S = 11.977, R-Sq = 99.0%, R-Sq (adj) = 98.8%, PRESS = 4973.44, R-Sq (pred) = 98.46%

Durbin-Watson statistic = 2.239

Table D.8 Analysis of variance

Source	DF	SS	MS	F	P
Regression	3	318689	106230	740.53	0.000
Residual Error	23	3299	143		
Total	26	321988			

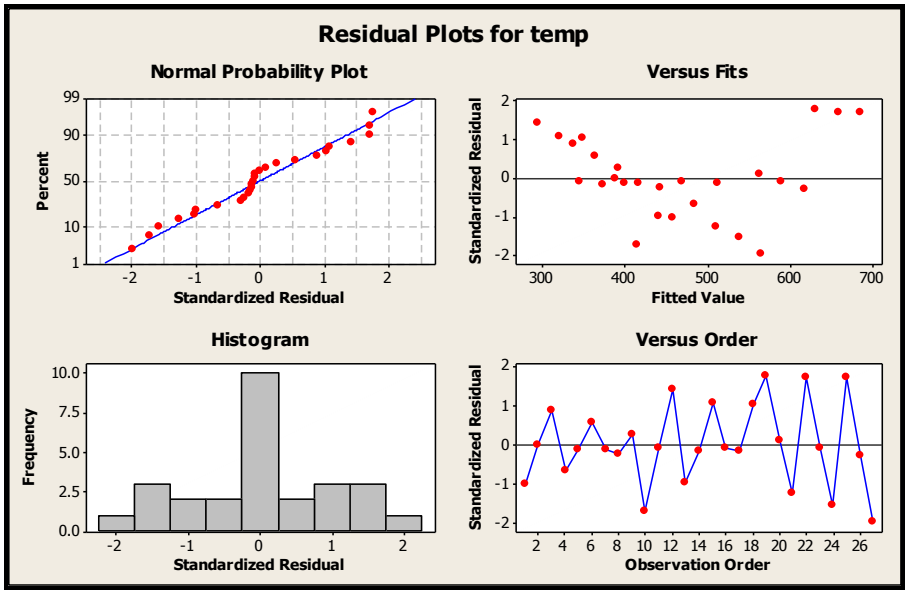

Figure D.4 LAFSW residuals plot for work piece temperature-304L stainless steel

Appendix E: Multiple Non Linear Regression Results

E.1 FSW of Aluminum Alloy-2195: Datafit Results

Model Definition: **Y = exp (a*x1+b*x2+c*x3+d)**

The regression equation is: $Y = \exp(0.0005012 * Q - 0.114 * v - 0.01637 * \phi + 5.82)$

Table E.1 Regression variable results

Variable	Value	Standard Error	t-ratio	Prob (t)
a	0.000501	0.0000378	13.24	0.0
b	-0.114	0.00526	-21.63	0.0
c	-0.0163	0.00172	-9.50	0.0
d	5.82	0.076	75.825	0.0

Table E.2 Non linear regression summary statistics

Sum of Residuals	1.36
Average Residual	0.0759
Residual Sum of Squares (Absolute)	1313.69
Residual Sum of Squares (Relative)	1313.69
Standard Error of the Estimate	9.686
Coefficient of Multiple Determination	0.982
Adjusted coefficient of multiple determination $R^2{}_{adj}$	0.978
Durbin-Watson statistic	2.822

Table E.3 Variance analysis

Source	DF	Sum of Squares	Mean Square	F Ratio	Prob(F)
Regression	3	72054.23	24018.07	255.96	0
Error	14	1313.69	93.835		
Total	17	73367.92			

E.2 FSW of 304L Stainless Steel: Datafit Results

Model Definition: **Y = exp (a*x1+b*x2+c*x3+d)**

The regression equation is: $Y = \exp(-0.1586 * v + 0.000691 * Q + 0.0764 * \phi + 5.65)$

Table E.4 Regression variable results

Variable	Value	Standard Error	t-ratio	Prob(t)
a	-0.1586	0.00618	-25.63	0.0
b	0.00069	0.0000	28.17	0.0
c	0.0076	0.0025	3.02	0.009
d	5.65	0.0543	103.92	0.0

Table E.5 Non linear regression summary statistics

Sum of Residuals	-0.544
Average Residual	-0.0302
Residual Sum of Squares (Absolute)	2421.98
Residual Sum of Squares (Relative)	2421.98
Standard Error of the Estimate	13.15
Coefficient of Multiple Determination	0.990
Adjusted coefficient of multiple determination R^2_{adj}	0.9884
Durbin-Watson statistic	2.73

Table E.6 Variance analysis

Source	DF	Sum of Squares	Mean Square	F Ratio	Prob(F)
Regression	3	251905.81	83968.60	485.37	0
Error	14	2421.98	172.99		
Total	17	254327.79			

E.3 LAFSW of Aluminum Alloy-2195: Datafit Results

Model Definition: **Y = exp (a*x1+b*x2+c*x3+d)**

The regression equation is: $Y = \exp(-0.0954 * v + 0.000533 * Q_{FSW} + 0.000357 * Q_{laser} + 5.260)$

Table E.7 Regression variable results

Variable	Value	Standard Error	t-ratio	Prob(t)
a	-0.09538	0.0029	-32.42	0.0
b	0.00053	0.0000	27.66	0.0
c	0.00036	0.0000	18.62	0.0
d	5.260489	0.0265	198.69	0.0

Table E.8 Non linear regression summary statistics

Sum of Residuals	-0.00548
Average Residual	-0.000202
Residual Sum of Squares (Absolute)	720.374
Residual Sum of Squares (Relative)	720.374
Standard Error of the Estimate	5.596
Coefficient of Multiple Determination	0.990
Adjusted coefficient of multiple determination R^2_{adj}	0.988
Durbin-Watson statistic	1.60

Table E.9 Variance analysis

Source	DF	Sum of Squares	Mean Square	F Ratio	Prob(F)
Regression	3	69938.0903	23312.6968	744.3243638	0
Error	23	720.3741	31.3206		
Total	26	70658.4644			

E.4 LAFSW of 304L Stainless Steel: Datafit Results

Model Definition: **Y = exp (a*x1+b*x2+c*x3+d)**

The regression equation is: $Y = \exp(0.00089 * Q_{FSW} + 0.000563 * Q_{laser} - 0.130 * v + 5.51)$

Table E.10 Regression variable results

Variable	Value	Standard Error	t-ratio	Prob(t)
a	0.00089	0.0000133	66.90939379	0.0
b	0.000563	0.0000368	15.2926326	0.0
c	-0.12932294	0.00365	-35.3829172	0.0
d	5.507119655	0.0217	254.329678	0.0

Table E.11 Non linear regression summary statistics

Sum of Residuals	-1.78438
Average Residual	-0.06608
Residual Sum of Squares (Absolute)	1270.910
Residual Sum of Squares (Relative)	1270.910
Standard Error of the Estimate	7.4335
Coefficient of Multiple Determination (R^2)	0.9960
Adjusted coefficient of multiple determination R^2_{adj}	0.9955
Durbin-Watson statistic	1.72945

Table E.12 Variance analysis

Source	DF	Sum of Squares	Mean Square	F Ratio	Prob(F)
Regression	3	320717.510	106905.836	1934.703	0
Error	23	1270.9097	55.25694730		
Total	26	321988.4200			

Vita

Shivani Daftardar was born in Pune, India, on March 11, 1983. She joined the Mechanical Engineering Department at Maharashtra Institute of Technology in India, and received the degree of Bachelor of Engineering in 2005. Interested in optimizing processes and lean manufacturing techniques, she chose Industrial Engineering as her major, and joined the Department of Industrial Engineering at Louisiana State University in August 2006. With a mechanical engineering background, she began working on finite volume modeling and metaheuristics under the supervision of Dr. T Warren Liao. The degree of Master of Science in Industrial Engineering will be conferred at the May 2009 commencement.